ARMY RESEARCH LABORATORY

Distributed Fiber-Optic Sensing and Numerical Simulation of Shock Wave Response of Manufactured Clay

Phase I: Software Model

Sibel Pamukcu, Clay Naito, Mesut Pervizpour, Qingsong Cui, Patrick A. Trasborg, Carlos Medina, and Mark A. Mentzer

ARL-TR-6399 **April 2013**

NOTICES

Disclaimers

The findings in this report are not to be construed as an official Department of the Army position unless so designated by other authorized documents.

Citation of manufacturer's or trade names does not constitute an official endorsement or approval of the use thereof.

Destroy this report when it is no longer needed. Do not return it to the originator.

Army Research Laboratory
Aberdeen Proving Ground, MD 21005-5068

ARL-TR-6399 **April 2013**

Distributed Fiber-Optic Sensing and Numerical Simulation of Shock Wave Response of Manufactured Clay

Phase I: Software Model

Sibel Pamukcu, Clay Naito, Mesut Pervizpour, Qingsong Cui, and Patrick A. Trasborg
Civil and Environmental Engineering Department, Lehigh University

Carlos Medina
Hayward Baker, Inc.

Mark A. Mentzer
Survivability/Lethality Analysis Directorate, ARL

REPORT DOCUMENTATION PAGE	Form Approved OMB No. 0704-0188

1. REPORT DATE *(DD-MM-YYYY)*	2. REPORT TYPE	3. DATES COVERED (From - To)
April 2013	Final	1 January 2010–1 June 2010

4. TITLE AND SUBTITLE
Distributed Fiber-Optic Sensing and Numerical Simulation of Shock Wave Response of Manufactured Clay Phase I: Software Model

5a. CONTRACT NUMBER

5b. GRANT NUMBER

5c. PROGRAM ELEMENT NUMBER

6. AUTHOR(S)
Sibel Pamukcu,[*] Clay Naito,[*] Mesut Pervizpour,[*] Qingsong Cui,[*] Patrick A. Trasborg,[*] Carlos Medina,[†] and Mark A. Mentzer[‡]

5d. PROJECT NUMBER

5e. TASK NUMBER

5f. WORK UNIT NUMBER

7. PERFORMING ORGANIZATION NAME(S) AND ADDRESS(ES)
U.S. Army Research Laboratory
ATTN: RDRL-SLB-W
Aberdeen Proving Ground, MD 21005-5068

8. PERFORMING ORGANIZATION REPORT NUMBER
ARL-TR-6399

9. SPONSORING/MONITORING AGENCY NAME(S) AND ADDRESS(ES)

10. SPONSOR/MONITOR'S ACRONYM(S)

11. SPONSOR/MONITOR'S REPORT NUMBER(S)

12. DISTRIBUTION/AVAILABILITY STATEMENT
Approved for public release; distribution is unlimited.

13. SUPPLEMENTARY NOTES
[*]Civil and Environmental Engineering Department, Lehigh University, Bethlehem, PA 18015
[†]Hayward Baker, Inc., 16 Drumlin Drive, Weedsport, NY 13166
[‡]U.S. Army Research Laboratory, Aberdeen Proving Ground, MD 21005-5068

14. ABSTRACT
The main objective of the proposed work was to determine the efficacy of distributed fiber-optic sensing in the form of Brillouin Optical Time Domain Reflectometry/Analysis and/or fiber Bragg grating application to measure and model the spatial and temporal distribution of dynamic strains in a bed of manufactured clay in response to an applied impact load at its surface.

15. SUBJECT TERMS
fiber sensor system, clay-backed testing, behind-armor blunt trauma, BOTDR, BOTDA

16. SECURITY CLASSIFICATION OF:			17. LIMITATION OF ABSTRACT	18. NUMBER OF PAGES	19a. NAME OF RESPONSIBLE PERSON
a. REPORT	b. ABSTRACT	c. THIS PAGE			Mark A. Mentzer
Unclassified	Unclassified	Unclassified	UU	48	19b. TELEPHONE NUMBER (*Include area code*) 410-278-3599

Standard Form 298 (Rev. 8/98)
Prescribed by ANSI Std. Z39.18

Contents

List of Figures

List of Tables

Preface

The main objective of the proposed work was to determine the efficacy of distributed fiber-optic sensing in the form of Brillouin Optical Time Domain Reflectometry/Analysis (BOTDR/ BOTDA) and/or fiber Bragg grating (FBG) application to measure and model the spatial and temporal distribution of dynamic strains in a bed of manufactured clay in response to an applied impact load at its surface.

Objectives

The specific objectives were to:

A. Characterize the test clay and establish the essential constitutive model parameters through a series of laboratory tests.

B. Conduct a three-dimensional (3-D) finite element analysis (FEA) of a representative clay bed model of given boundary and initial conditions and the established constitutive model parameters to simulate the evolution of the internal stress-strain distribution and the deformed shape of the clay upon impact load. ABAQUS and/or SAP (FEA tools) were to be utilized to conduct this analysis.

C. Measure the two-dimensional (2-D) (lateral) dynamic stress-strain distribution at a strategically selected plane of the clay bed in response to a simulated impact load applied orthogonal to its surface. Compute the vertical stress-strain distribution using the Poisson's constant and/or the lateral earth pressure coefficient of the packed clay.

D. Measure the 2-D (lateral) evolution of stress-strain distribution on multiple internal parallel planes inside the clay bed to create a 3-D representation of the behavior.

E. Conduct baseline measurements of sensor signal and the evolution of the stress-strain distribution profiles with temperature as it increases from room temperature (21 ºC) to a select elevated temperature (71.1 ºC).

F. Conduct measurements of the evolution of the stress-strain distribution profiles over time, starting at completion of the impact load to a select time determined by the thixotropic strength gain behavior of the clay.

G. Facilitate pre-impact and post-impact imaging of the interior of the clay containing the embedded fiber to determine potential separation of fiber from clay matrix and/or its slippage from the original lay-out pattern.

H. Conduct a comparative analysis between the measurements made by the fiber-optic sensor arrays and the results of the numerical simulations, followed by a parameter verification to calibrate the model.

I. Conduct a mathematical or a numerical procedure to determine the time history of loading—impact impulse function—using the measured strain distribution and the deformed shape of the clay bed after a single impact. New appropriate software may be needed or developed to meet this objective.

Requirements

The program plan was to comply with the following requirements:

1. All of the required optics equipment and other items needed for testing and characterization will be procured by the project owner, Aberdeen Test Center (ATC), and loaned to Lehigh University. All pretest and posttest imaging of the test box will be conducted by ATC laboratories as needed.

2. Steps toward technology transfer to ATC will be taken toward the end of a 12-month period of bench and floor-scale testing at Lehigh University.

3. The models and any associated software created and used for the purposes of this project will be shared with ATC free of any additional fees or licensing.

4. All proposed publications of the results of this work will be subject to review and approval through ATC internal protocols (operational security) prior to their release.

5. The program will follow three phases with progress reports and deliverables as described in the following sections:

    • Phase I. Software Model

    • Phase II. Breadboard

    • Phase III. Brassboard.

Project Plan

The outline of the tasks and the deliverables to achieve the specific objectives stated earlier is as follows:

Phase I. Software Model

Task 1. Conduct a series of characterization tests to measure the physical, mechanical, and constitutive properties of the test clay. The physical properties to be determined are: water content/void ratio, mass density, and plasticity indices. The mechanical and constitutive properties to be determined are: thixotropic behavior with time, compression and distortion parameters, dynamic and static elastic constants (E, G, and ν, respectively); lateral earth pressure coefficient; and variation of the elastic constants and stress-strain behavior with loading rate and elevated temperatures from room temperature.

Task 2. Construct a 3-D numerical model of the clay bed with five rigid boundaries and one flexible boundary on the top surface using ABAQUS and/or SAP tools. Selection of the appropriate FEA tool will be determined based on the capability to provide the best simulation of the impact loading of the test specimen.

Task 3. Apply the simulation model to analyze its sensitivity to various input parameters, including material properties, boundary, and initial conditions, and solve for the temporal and spatial distribution of internal stress and strains in the clay bed in response to a design impact load of a predetermined period and time history. Obtain the deformed shape of the clay at select intervals of the time history of loading.

Phase II. Breadboard

Task 1. Select, design, and test a BOTDR/BOTDA or FBG photonics data acquisition system capable of acquiring distributed strains as a result of an estimated 200-μs duration dynamic (impact) load. The goal is to acquire distributed data over the linear positioning of the fiber for a maximum spatial resolution of 1 m, a maximum temporal resolution of 10 μs, and a measurement accuracy of 1 μs.

Task 2. Design and construct the first test specimen (T1), a laterally confined clay bed 24 × 24 × 6 in, with the optical fiber embedded at a strategic horizontal plane within the test clay. The fiber will be placed in a grid pattern, enabling localized measurement confirmation at two distinct points on its linear positioning. (Figure P-1 provides a conceptual schematic of the T1 setup.) Select a suitable method of simulating impact loading on the clay surface.

Task 3. Conduct baseline measurements for pretest static conditions, that is, null measurements of the unstrained fiber in clay in its in-situ grid configuration at room temperature (21 °C) and at two other elevated temperatures between 21 °C and 71.1 °C. Design and construct the bench-top facility to increase and keep the temperature of the test clay to a constant level during testing.

Task 4. Conduct impact load tests within selected time intervals (i.e., 3-min intervals) and record multiple series of strain data at three selected constant temperatures (i.e., 21 °C, 46 °C, and 71.1 °C).

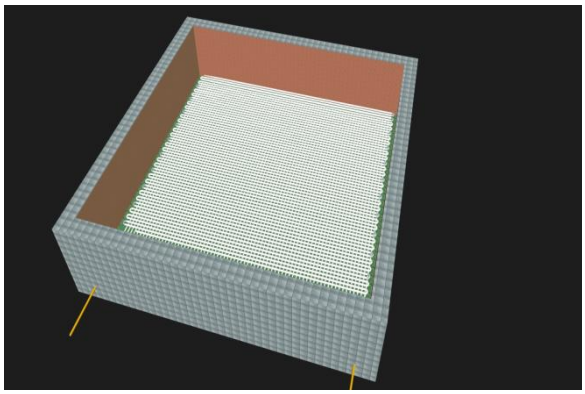

Figure P-1. Clay bed test box with fiber-optic grid layout at the bottom of the box for T1 specimen.

Task 5. Conduct strain measurements at select intervals of time duration after the completion of each series of impact load tests to assess the influence of thixotropic behavior of the clay. Continue these time interval measurements until reaching a predetermined time of thixotropic strength gain of the test clay.

Task 6. Design and construct the second test specimen (T2), a laterally confined clay bed 24 × 24 × 6 in, with the optical fiber embedded throughout the entire depth of the clay. The fiber layout will follow the same grid pattern established in T1, with the fiber contained in multiple parallel planes starting at the bottom surface and repeated at every 1-in lift of clay. (A conceptual schematic is provided in figure P-2.)

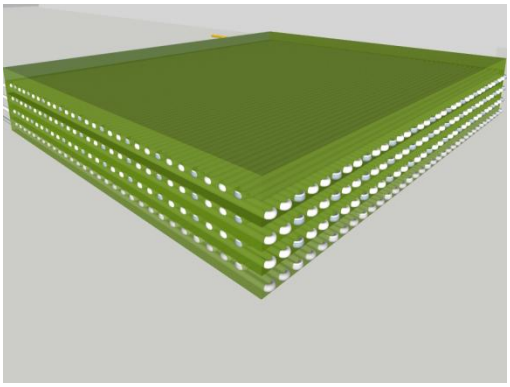

Figure P-2. Parallel plane fiber-optic grid layout for T2 specimen.

Task 7. Compare the strain measurements of T1 and T2 specimens with the numerical results obtained from FEA and calibrate the model using the test results. The model calibration step (C1) in this task will constitute adjustment of input material characteristics and the boundary and initial conditions as necessary. Iterative corrections to the estimated

vertical strains from lateral strain measurements may be necessary if any temporal and spatial changes in the material properties of the clay are considered during and after impact loading.

Task 8. Evaluate the time history or impact impulse function using the actual measurements of the time evolution of the strain field in the test clay bed upon impact. Use the evaluated function to conduct a second step calibration (C2) of the model.

Phase III. Brassboard

Task 1. Set up a floor-scale test facility to simulate impact load using an air-gun facility on the fiber instrumented test clay. Compare strain distribution measurements with previous test results and calibrate the numerical model as necessary.

Task 2. Assist in repeating the floor-scale experiments at ATC facilities using the design impact loading. Compare the strain distribution measurements and calibrate the numerical model as necessary.

Task 3. Assist in establishing preliminary test protocols for technology transfer and potential standardization of data acquisition from fiber instrumented test clay.

Table P-1 shows the proposed work over the course of 12 months.

Table P-1. Project schedule.

Time	First Quarter			Second Quarter			Third Quarter			Fourth Quarter		
PHASE I												
Task 1												
Task 2												
Task 3												
PHASE II												
Task 1												
Task 2												
Task 3												
Task 4												
Task 5												
Task 6												
Task 7												
Task 8												
PHASE III												
Task 1												
Task 2												
Task 3												
REPORT												

INTENTIONALLY LEFT BLANK.

1. Summary

This report presents the results of a series of material characterization tests conducted to determine the essential constitutive model parameters for a three-dimensional finite element simulation and the preliminary results of the constructed numerical model. The model was solved to predict the temporal strain profiles in a body of manufactured clay—Roma Plastilina Clay No. 1—subjected to a single impact force typical of those generated using National Institute of Justice (NIJ) Standard 10101.04 *Ballistic Resistance of Personal Body Armor* (*1*). Using the baseline material properties of undisturbed clay, the model predicted maximum back face signature (BFS) of
21.3 mm, which is comparable to the expected standard of 19.0 ± 2.0 mm from the NIJ calibration (ball-drop test) of properly prepared test clay.

Although the model was able to capture the allowable BFS with the specific undisturbed clay parameters (Drucker-Prager) imposed, the strain profile varies significantly through the depth of the clay bed due to the flexibility and yield properties of the clay. The magnitude of this strain profile is important for the arrangement and resolution of the fiber-optic gauge array intended to measure the internal strains. The ultimate goal is to determine a location and quantity of fiber to be used that will not affect the BFS of the shot at the failure level while still providing adequate strain resolution. Accurate prediction of the strain profiles, the BFS, and, subsequently, the impact load history (impulse energy function) requires input selection of realistic constitutive parameters and a yield model.

Continuing material characterization tests have indicated that, unlike the undisturbed clay, the temperature equilibrated and remolded clays behave more like the Cam-Clay or von Mises model material, i.e., displaying no volume change upon yield, than the frictional solid of the Drucker-Prager model. Tests also showed that the elastic and yield properties of the clay are strain-rate dependent and that the clay displays thixotrophic stiffness gain with time. Improved modeling efforts that take these factors into consideration are being continued, accompanied by better understanding of the complex mechanics of the remolded clay at room (73 °F) and elevated temperatures (105 °F).

INTENTIONALLY LEFT BLANK.

2. Overview

The main objective of this project is to determine the efficacy of distributed fiber-optic sensing in the form of Brillouin Optical Time Domain Reflectometry/Analysis (BOTDR/BOTDA) and/or fiber Bragg grating (FBG) application to measure and model the spatial and temporal distribution of dynamic strains in a bed of manufactured clay (Roma Plastilina [RP] Clay No. 1) in response to an applied impact force on its surface.

The proposed outline of the tasks and the deliverables to achieve the specific objectives of phase I is as follows:

2.1 Task 1. Material Characterization

Conduct a series of characterization tests to measure the physical, mechanical, and constitutive properties of the test clay. The physical properties to be determined are water content/void ratio, mass density, and plasticity indices. The mechanical and constitutive properties to be determined are: thixotrophic behavior with time, compression and distortion parameters, dynamic and static elastic constants (E, G, and ν, respectively); lateral earth pressure coefficient; and variation of the elastic constants and the stress-strain behavior with loading rate and elevated temperatures from room temperature.

2.2 Task 2. Construction of Numerical Model

Construct a three-dimensional (3-D) numerical model of the clay bed with five rigid boundaries and one flexible boundary on the top surface using ABAQUS software.

2.3 Task 3. Analysis of Model

Apply the simulation model to analyze its sensitivity to various input parameters, including material properties and boundary and initial conditions, and solve for the temporal and spatial distribution of internal stress and strains in clay bed in response to a design impact load of a predetermined period and time history. Obtain the deformed shape of the clay at select intervals of the time history of loading.

Phase I of the project involved laboratory determination of the essential constitutive model parameters for a 3-D finite element analysis (FEA). The FEA model was developed to simulate the evolution of the internal stress-strain distribution and the deformed shape upon impact load onto a clay bed of given boundary and initial conditions and material properties. A mathematical procedure is proposed to determine the impulse energy function. This procedure relies on using the verified simulated relationship between a characteristic strain profile and the surface pressure imparted on the clay. This procedure will be tested and calibrated using the fiber-optic measured strain distributions in the next two phases of the continuing project.

3. Methods and Materials

3.1 Task 1: Material Characterization of Roma Plastilina (RP) No.1 Clay

3.1.1 Types of Tests

Various laboratory tests are conducted to quantify the behavior of the RP clay. Load-deformation response is investigated through deformation-controlled (large-strain) and load-controlled (constrained) compression tests. The impact of strain rate is investigated by large-strain compression tests. Evidence of thixotrophic behavior is determined through nondestructive small-strain tests. The thermal diffusivity coefficient and the time duration required for thermal equilibration are determined through heating and cooling tests.

The reported tests are conducted on both undisturbed (pristine clay bricks) and remolded samples. All material characterization essential for the initial numerical model studies reported in this report were conducted at room temperature. The mechanical properties at elevated temperatures (105 °F) and thermally equilibrated conditions are continuing at the time of this report, so their results are not reported. The results of ball-drop tests (*1*) will be reported in conjunction with the fiber-optic measurements of the next phase of the project, and thus are not included in this report. Table 1 presents the type of tests completed/continuing and the associated parameters and properties measured. Table 2 provides the description of the parameters listed in table 1.

Table 1. The tests conducted and the parameters measured for characterization of RP clay.

Test Type		Temperature (°F)		Duration	Rate	Status[a]	
		Room (R) (73.5 °F)	Elevated (E) (105 °F)			R	E
A. Small-strain (nondestructive)		G, E, ν	G, E, ν	Can be repeated for thixotrophy	Independent	√	∞
B. Large-strain compression		σ_{max}, E_{sec}, φ (β), c (d)	σ_{max}, E_{sec}, φ (β), c (d)	Variable from hours to days	0.1–50 mm/min	√	∞
B1. Uniaxial	B2. Triaxial						
C. Constrained compression		M, λ, κ	M, λ, κ	Days	Independent	√	∞
D. Thermal diffusivity		α_t		Hours	Independent	—	∞/√

[a] ∞ = continuing; √ = completed.

Table 2. Description of the parameters listed in table 1.

Parameter Designation	Description	Notes
G	Shear modulus	Maximum or initial modulus
E	Elastic or Young's modulus	Maximum or initial modulus
ν	Poisson's ratio	—
σ_{max}	Maximum axial stress	Deviatoric stress at failure
E_{sec}	Secant modulus at yield strain	Yield strain correspond to maximum axial stress
M	Constrained modulus	Initial tangent to constrained stress-strain compression curve
φ (β)	Internal friction angle	β = designation of friction term in model
c (d)	Cohesion	d = designation of cohesion term in model
λ	Load modulus	Volumetric compression index
κ	Unload modulus	Rebound index
α_t	Coefficient of thermal diffusivity	Describes rate of heat conduction

3.1.2 Sample Preparation

The uniaxial and the triaxial compression tests of the RP clay were conducted using standard cylindrical samples with a diameter of 72 mm and height of 144 mm. The undisturbed cylindrical samples were trimmed to size from the pristine clay bricks. The remolded cylindrical samples were prepared by first rolling clay to a thin flat sheet, which was rolled into a rod and coiled into a disc to completely fill the cylindrical sample mold in layers, as shown in figure 1. A standard Proctor hammer was used to deliver a predetermined constant energy on each layer of coiled clay. The sample was completed in five layers with 10 blows per layer. The surface of each compacted layer was scratched to assure binding between layers. The sample was then left to sit for 1 h to gain sufficient consistency before removal from the mold. The surface of the sample was smoothened as needed. The remolded samples were stored at room temperature for 24 h and tested the next day. The consecutive stages of sample preparation and the standard compaction energy calculations are shown in figure 1.

The thermally conditioned samples were first remolded as previously described. They were then placed in the oven for 8 h at a constant temperature of 105 °F and tested immediately upon removal from the oven. The one-dimensional, laterally constrained compression tests were conducted on disk-shaped samples with an initial height of 25.4 mm and diameter of 63.5 mm. These sample discs were trimmed from the mid-height of one-day-old remolded cylindrical samples.

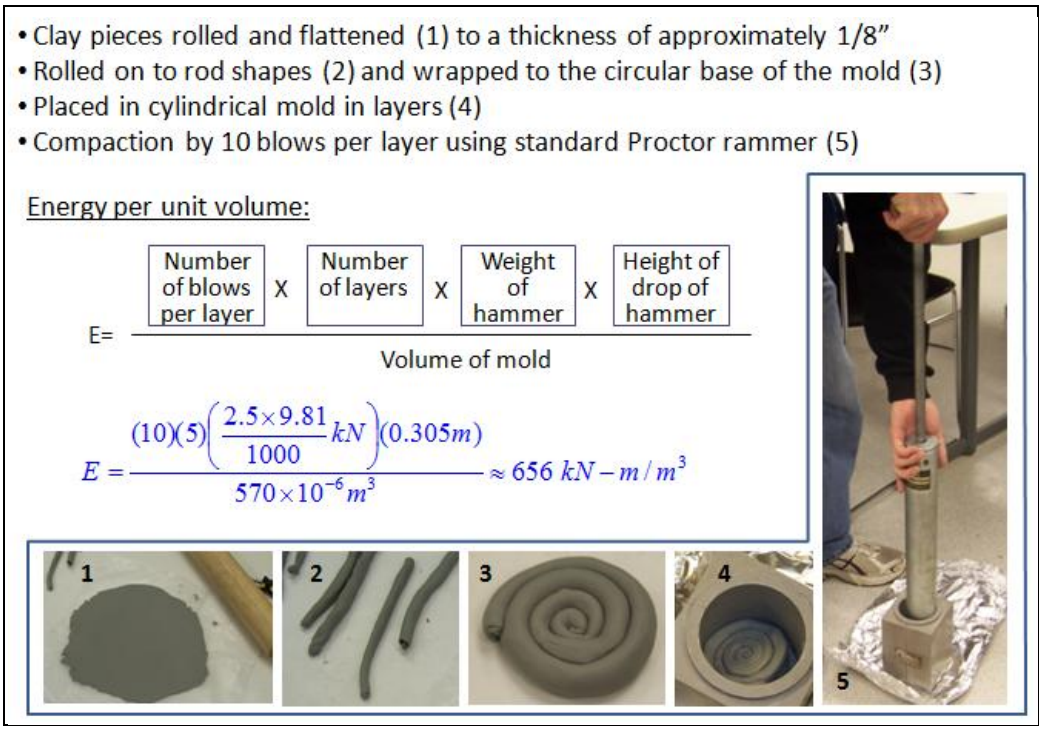

Figure 1. Preparation of remolded sample and the standard energy calculation.

3.1.3 Description of Tests

3.1.3.1 A. Small-Strain Tests (Ultrasonic Wave Velocity)

A nondestructive ultrasonic test method (figure 2) is utilized to measure time of arrival of primary (P) and shear (S) waves to detect temporal variation of the elastic properties upon remolding. The P- and S-wave velocities are calculated from arrival times and the length of wave path along the thickness of test sample. The calculation of Young's modulus (E), shear modulus (G), and the Poisson ratio (υ) employ the following expressions:

$$G = \rho V_s^2, \tag{1}$$

$$E = \frac{\rho V_p^2 (1+\upsilon)(1-2\upsilon)}{(1-\upsilon)}, \tag{2}$$

and

$$\upsilon = \frac{1-2\left(V_s/V_p\right)^2}{2-2\left(V_s/V_p\right)^2}, \tag{3}$$

where:

ρ = mass density of clay (kg/m^3),

υ = Poisson ratio,

V_s = shear wave velocity (m/s),

V_p = primary wave velocity (m/s),

G = Shear modulus (Pa), and

E = Young's modulus (Pa).

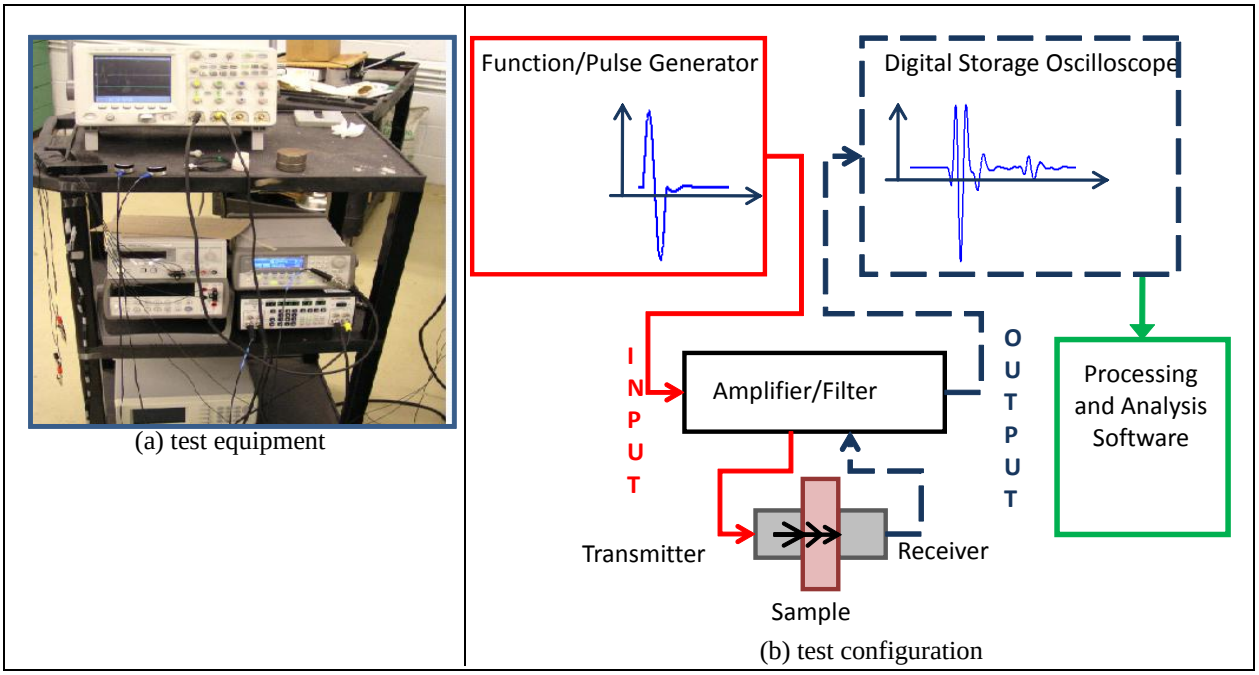

Figure 2. Ultrasonic wave propagation measurement.

3.1.3.2 B. Large-Strain Compression Tests

Stress-strain response is obtained from uniaxial (unconfined) compression and triaxial compression tests conducted on cylindrical clay samples encased in a fluid-tight membrane.

3.1.3.2.1 B1. Uniaxial (Unconfined) Compression Test (*ASTM D2166-06*) (*2*). Uniaxial compression of cylindrical samples is conducted on undisturbed, remolded, and thermally conditioned samples in deformation rates ranging from 0.1 to 50 mm/min (figure 3). In these tests, a constant-rate axial deformation is applied under zero confining stress. The uniaxial compression test provides direct calculation of Young's modulus (E, initial slope), yield stress (σ_y, transition from elastic to plastic behavior), and maximum stress (σ_{max}, peak true stress at failure), as depicted in figure 4.

(a) Test equipment

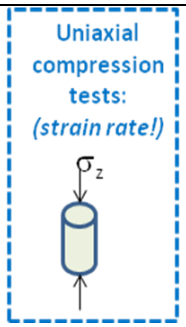

(b) Test configuration

Figure 3. Unconfined compression testing (ASTM D2166-06).

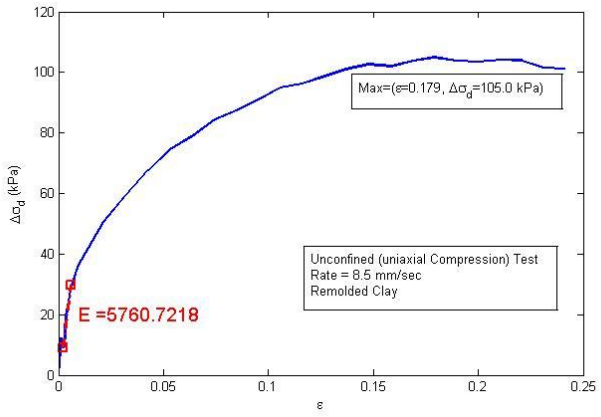

(a) Typical measured stress-strain response

$$E = \frac{d\sigma_z}{d\varepsilon_z}$$

(b) Computation of initial modulus

Figure 4. Typical test data obtained from axial compression tests

3.1.3.2.2 B2. Triaxial Compression Test (*ASTM D2850-03a*) (*3*). Triaxial compression apparatus allows the application of two independently controlled stresses on a test sample. The specimen is loaded to a preselected hydrostatic confining pressure (σ_3). The confining pressure is then held constant while the axial deformation is applied at a constant rate (figure 5). The applied axial strain induces increments of axial stress (deviatoric stress) above the confining pressure, which results in shear stresses on all planes within the sample except the principal directions. The dependence of the material shear strength on normal stresses can be tested in this manner. Testing multiple samples at different levels of confining pressure leads to the determination of the characteristic yield surface of the material at failure.

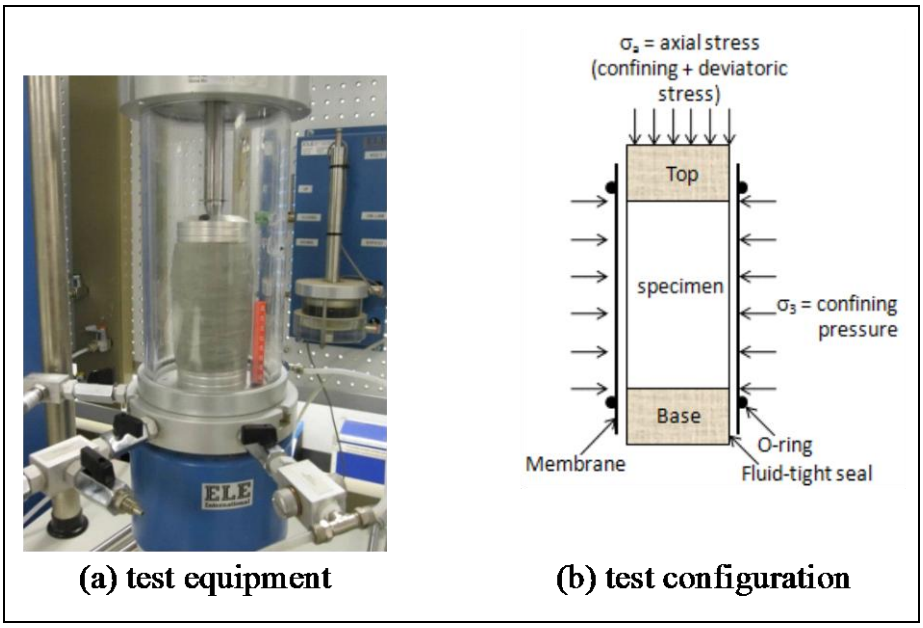

Figure 5. Triaxial compression testing (ASTM D2850-03a).

For these series of tests, cylindrical samples confined under hydrostatic pressures of 3.5, 7, 10.5, 14, 28, 69, and 138 kPa were loaded axially to failure under constant rates of deformation. The pairs of confining hydrostatic pressure and the deviatoric stress at failure are used to define the yield surface and strength properties of the clay. Typical shear strength parameters such as cohesion (c) and internal friction angle (ϕ) are used to define the Mohr-Coulomb failure model ($\tau_f = c + \sigma \tan\phi$). The shear and post-failure parameters are used in material description of various plasticity models (i.e., Drucker-Prager, Cam-Clay, and von Mises).

3.1.3.3 C. Constrained Compression Test (ASTM D2435-04) (*4*)

Laterally constrained (radial strain, $\varepsilon_r = 0$), disk-shaped samples (height = 25.4 mm, diameter = 63.5 mm) are tested under load-controlled conditions (figure 6). In these tests, a predefined set of loading and unloading steps are applied to the specimen following a given loading schedule, and the resulting axial deformation is recorded with time for each load-unload step. Due to the lateral constraint, the axial strain ε_z is equivalent to the volumetric strain ε_v at each load-unload step ($\varepsilon_v = \varepsilon_z$). The constrained elastic modulus (M) is calculated from the initial linear segment and slopes of unload/reload segments of the axial stress-strain plots, as shown in figure 7. The relationships between E, G, constrained (M) and bulk (K) modulus are computed as:

$$G = \frac{E}{2(1+\nu)},\ M = \frac{E(1-\nu)}{(1+\nu)(1-2\nu)},\ K = \frac{E}{3(1-2\nu)}. \quad (4)$$

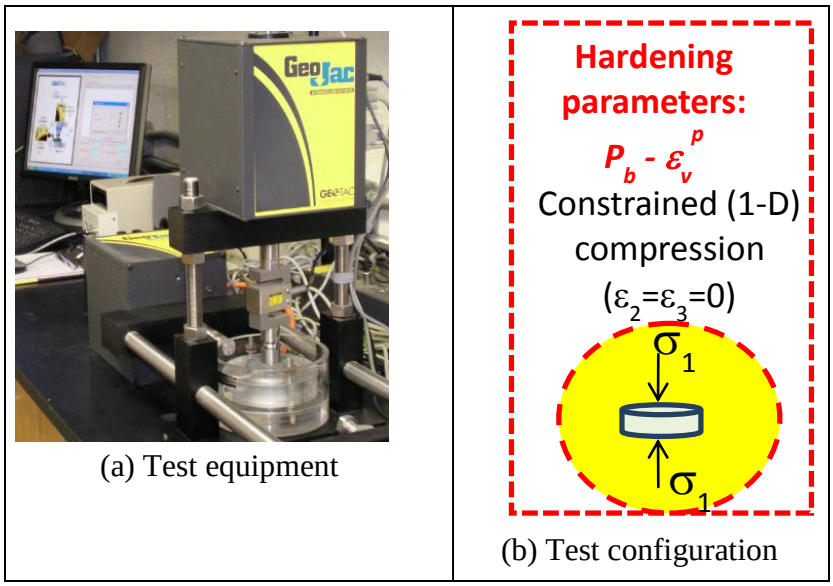

(a) Test equipment

(b) Test configuration

Figure 6. Constrained compression tests (ASTM D2435-04).

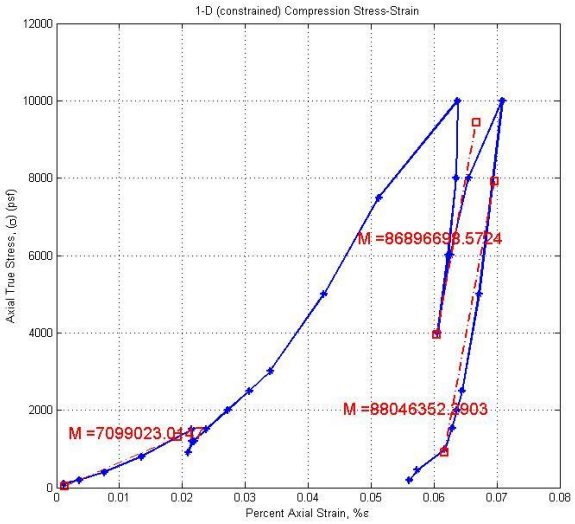

(a) True axial stress-axial strain in constrained testing

$$M = \left.\frac{d\sigma_z}{d\varepsilon_z}\right|_{\varepsilon_r=0}$$

(b) constrained modulus definition

Figure 7. Typical test data obtained from constrained compression tests.

The plot of the volumetric strain vs. natural logarithm of mean stress relation lead to the graphical computation of material plastic parameters λ and κ. Lambda (λ) is the slope of the virgin deformation curve representing the total deformation (= plastic + elastic) and kappa (κ) is the slope of the unload/reload segment of the curve representing the elastic deformation, as shown in figure 8. The yield stress and the hardening response of the material (pairs of stress and plastic strain data) can then be obtained from this plot, as depicted in figure 8b.

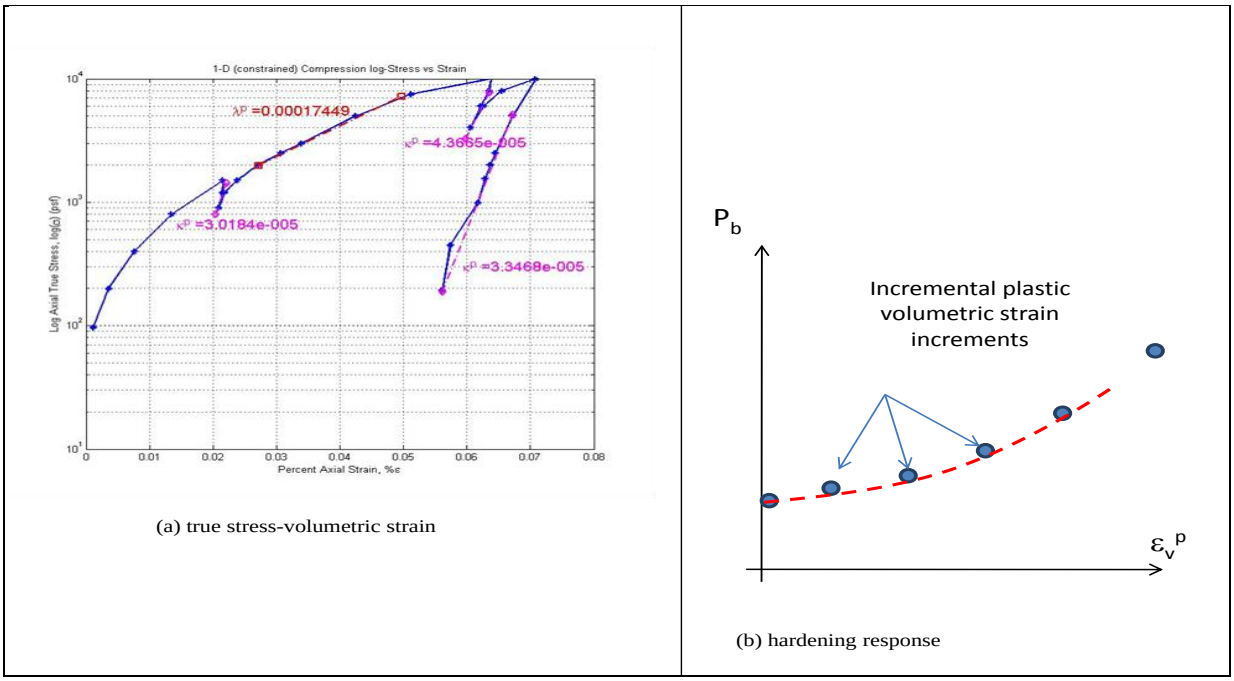

Figure 8. Typical plastic behavior data obtained from constrained compression tests.

3.1.3.4 D. Thermal Diffusivity Test

The period required for thermal equilibrium in the oven and cooling back to the room temperature once removed from the oven is a function of thermal diffusivity of the clay, the ratio of the convection coefficient of the environment, and the conduction coefficient of the specimen. The remolded cylindrical samples were thermal conditioned by first heating in a constant temperature oven at 105 °F and then cooling at a room temperature of 73.5 °F. The samples were instrumented with K-type thermocouples placed equidistant from the center to the surface of each cylinder. The ambient temperatures of the oven and the room were recorded by two additional thermocouples, as shown in figure 9.

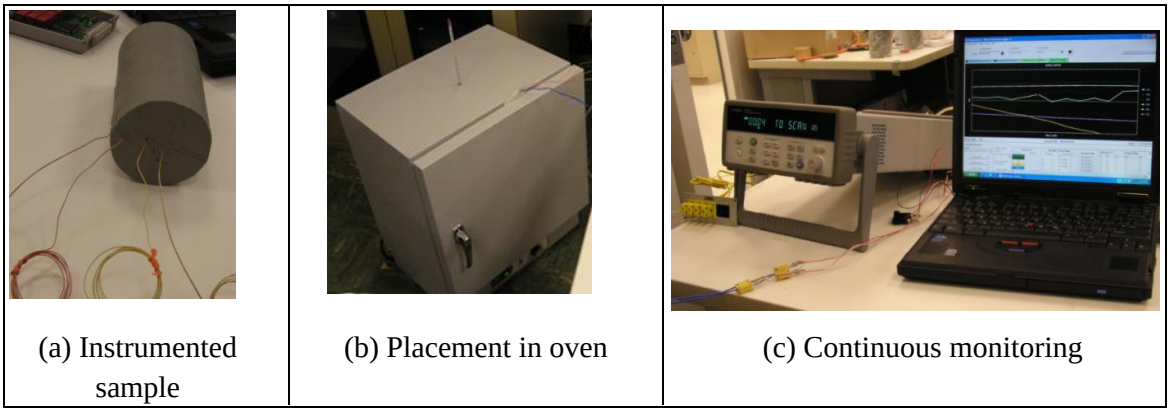

(a) Instrumented sample

(b) Placement in oven

(c) Continuous monitoring

Figure 9. Thermal conditioning of remolded clay samples.

The following governing energy conservation equation was solved numerically in cylindrical coordinates for a long cylinder subject to surface convection boundary conditions:

$$\frac{\partial T}{\partial t} = \alpha\left[\left(\frac{1}{r}\right)\frac{\partial T}{\partial r} + \frac{\partial^2 T}{\partial r^2} + \frac{\partial^2 T}{\partial z^2}\right], \tag{5}$$

where

r: radial distance of location from center (cm),

z: axial distance along the length (cm),

t: time(s),

T: temperature at a location and time T(r,t), and

α: Thermal diffusivity (cm^2/s).

The thermal diffusivity of the sample was computed by a parameter estimation approach using an optimization routine on a least square type objective function that describe the error term between the experimental and the simulated numerical responses.

3.2 Task 2 and Task 3: Construction and Analysis of Numerical Model

The finite element method (FEM) was utilized to model the response of the RP clay subjected to impact. The analysis problem lends itself to the FEM because the impact test is designed to not penetrate the clay body. ABAQUS version 6.9.1 is used for the research study. The "Explicit" version of the program is utilized to model the dynamic impact.

3.2.1 Review of the Plasticity Models

A brief overview of plasticity models for Modified Drucker-Prager, Modified Cam-Clay, and von Mises are provided here. Some of the common model stress parameters and their descriptions are as follows:

Table 3. Common model stress parameters.

$\Delta\sigma_d = \sigma_a - \sigma_3 = q$	Deviatoric (true) stress for cylindrical triaxial test ($\sigma_a=\sigma_1$= axial stress)
$p = (\sigma_a + 2\sigma_3) / 3$	True mean stress for cylindrical triaxial test

3.2.1.1 Modified Drucker-Prager Cap Model

This plasticity model is capable of representing stress history, stress path, dilatancy, and impact of intermediate stresses. The yield surface is represented in three sections: a linear shear failure surface (F_s), elliptical cap surface (F_c) intersecting the mean effective stress axis at right angle,

and a smooth transition zone between the cap and the failure surface, as depicted in figure 10. Linear elastic response is captured by the bulk modulus K, which increases as material undergoes compression. Onset of plastic response is defined by the failure surface (F_s) and the cap yield surface (F_c).

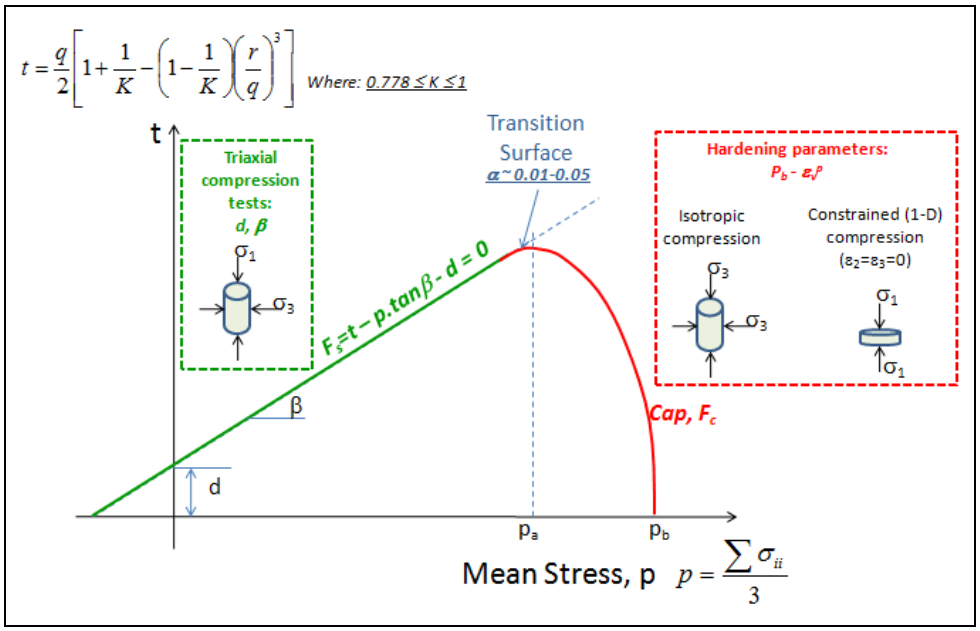

Figure 10. Drucker-Prager cap plasticity model, yield surface, and parameters.

The failure surface is obtained by tri-axial compression on samples at various levels of confining pressures. Slope of F_s (tanβ), represented by angle β and the intercept *d*, are the materials' angle of internal friction and cohesion in the p-t plane. The hardening (cap) yield surface (F_c) of the model is determined by conducting hydrostatic compression tests in a tri-axial compression device or one-dimensional laterally constrained tests. The results are expressed in terms of stress and volumetric plastic strains, as shown in figure 8.

3.2.1.2 Modified Cam-Clay

This model, based on the critical state theory of Schofield and Wroth (*5*), effectively predicts pressure-dependent strength and the compression and dilatancy for remolded clays. It states that the clay is continuously sheared until it flows as a frictional fluid at the critical state, where unlimited deformations without changes in stress or volume will occur at this state. The general parameter definitions are the mean stress (p) and the deviatoric stress (q), as previously provided. The critical state line (CSL) is expressed both in p-q and p-v space, where v is the specific volume. Accordingly,

$$qf = M' pf; v = \Gamma - \lambda' \ln(p), \quad (6)$$

where the slope of CSL in p-q space is M', the slope of the same line in v-lnp' space is λ', and Γ is the initial specific volume under unit pressure. The M' of CSL can be expressed in terms of internal friction angle φ, as M'= (6sinφ)/(3-sinφ).

3.2.1.3 Von Mises Model

Similar to the DP plasticity model, the von Mises model projection of the yield surface on to the π-plane is circular. However, unlike DP, which attains a conical failure surface in space, indicating failure stress grows as a function of confining pressure, the von Mises surface is cylindrical with constant cross-section, indicating that the failure stress is not a function of the confining stress, as shown in figure 11. The von Mises is represented when the internal friction angle of the material is very small, particularly observed for normally consolidated soft clays under rapid loading conditions.

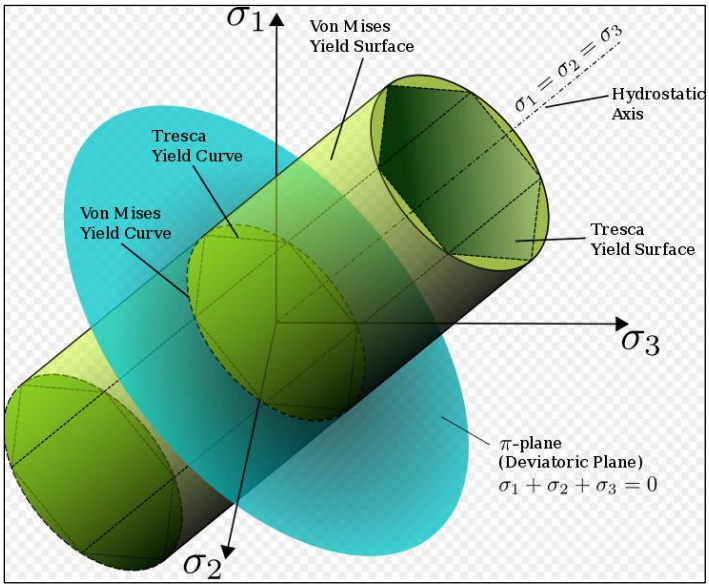

Figure 11. Von Mises yield criteria.

4. Results

4.1 Results of Task 1: Material Characterization of RP No. 1 Clay

Table 4 summarizes some of the pertinent index properties determined for RP clay.

Table 4. Measured index properties.

Property	Undisturbed Clay	Remolded Clay
Mass density (g/cm^3)	1.539	1.555
Moisture content/plasticity	NA (oil-based clay)	NA (oil-based clay)
Coefficient of thermal diffusivity (m^2/s)	2.1261×10^{-7}	

Note: NA = not applicable.

Note that the measured coefficient of thermal diffusivity of the RP clay material is relatively comparable to that of window glass (3.4×10^{-7} m^2/s) or rubber (1.3×10^{-7} m^2/s).

4.1.1 Small Strain Tests

The ultrasonic primary (P-wave) and shear wave (S-wave) propagations were conducted in megahertz and kilohertz frequency ranges. The undisturbed clay disc samples were 11.4 mm thick and the remolded samples 30.73 mm thick, all tested at room temperature. Table 5 lists the range of small strain parameters obtained for undisturbed samples. Figure 12 shows a typical pulse and output wave form and the computation of the wave velocity in these tests.

Table 5. Low strain test results of RP clay at room temperature.

Measured Property	Undisturbed
Vs, S-wave velocity (m/s)	616–832
Vp, P-wave velocity (m/s)	1550–1577
G, shear modulus (GPa)	0.6–1.0
E, Young's modulus (GPa)	1.6–3.0
ν, Poisson's ratio	0.406–0.307

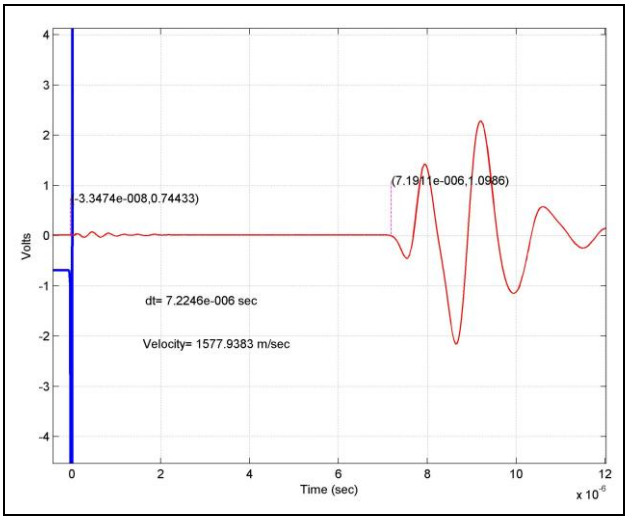

Figure 12. Sample pulse and output wave form.

The variation of P-wave velocities with time after remolded compaction of the clay is shown in figure 13. A clear increase is observed in the P-wave velocity with time. The increase is approximately 5% (from 1520 m/s to about 1600 m/s) for the first hour (53 min) and slightly over 1% for the next 7 h (492 min), as depicted by the bilinear approximation on the graph in figure 13. A quick check of the final value after 8 h (545 min) showed that the P-wave velocity stabilized at 1610 m/s, which is a few percent greater than the maximum undisturbed value indicated in table 5. These variations show that the material is prone to time-dependent strength and stiffness change. Similar tests are continuing to determine S-wave evolution with time.

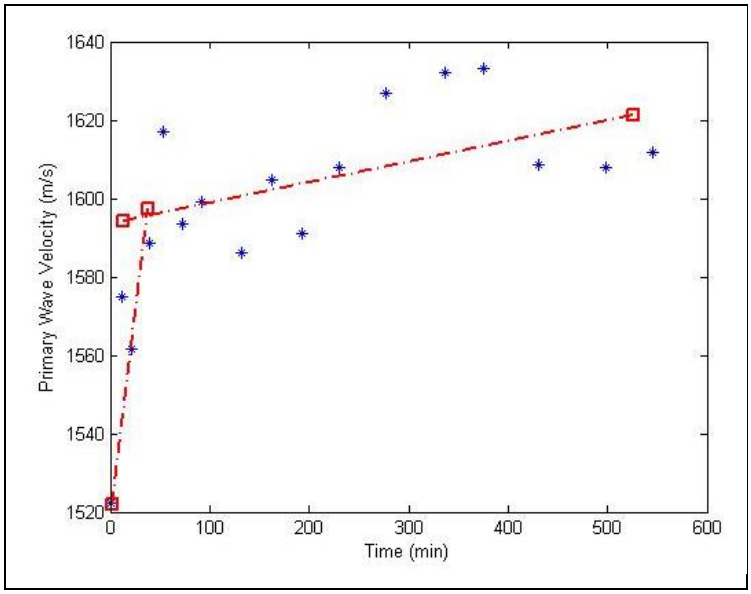

Figure 13. Variation of P-wave velocity with time after of remolding.

4.1.2 Large-Strain Compression Tests

4.1.2.1 B1. Uni-axial (Unconfined) Compression Test Results

These tests were conducted on both the undisturbed and the remolded samples at room temperature. Both type of samples displayed strain rate dependency of the maximum axial stress (σ_{max}) and stiffness (E_{sec}), as shown in figure 14. The results were compared to those determined by Munusamy and Barton (*6*) on the same RP clay. Table 6 displays the strength and stiffness values obtained and compared with the 2009 study. Also included in the table are the DP material model parameters computed and used in the numerical model of this study.

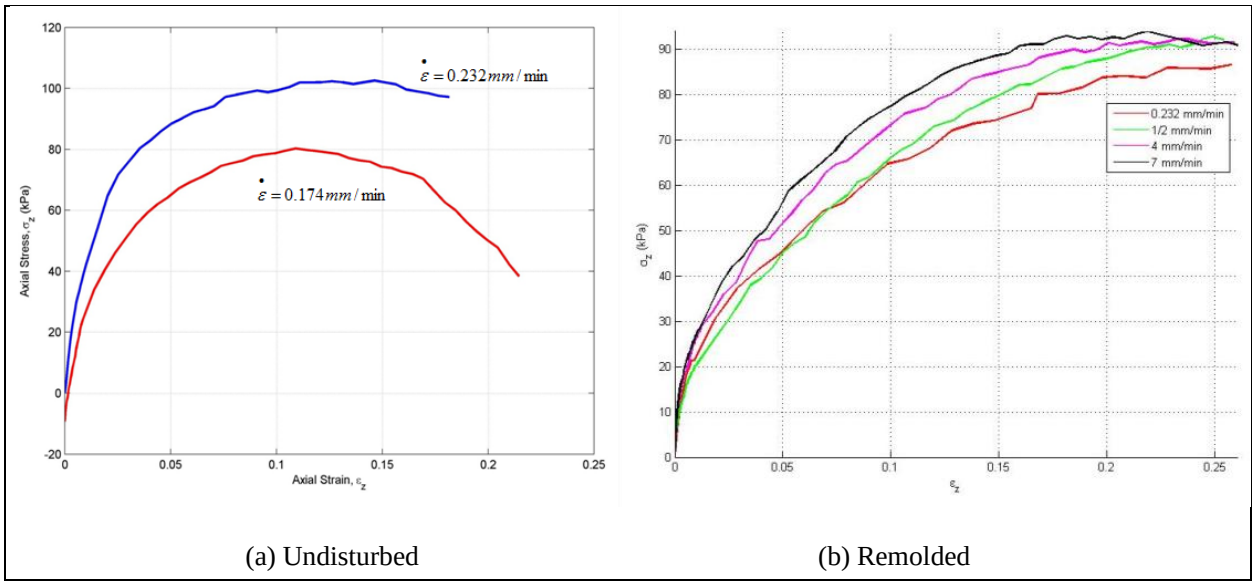

(a) Undisturbed (b) Remolded

Figure 14. Uni-axial compression of undisturbed and remolded samples.

Table 6. Uni-axial compression test results and Drucker-Prager model parameters.

Property	This Study			Munusamy and Barton 2009 study[b]
	Measured		Model Parameters	
	Undisturbed	Remolded		
E (low to high load rate)[a] MPa	4–9	4–10	6.58	—
E_{sec} (MPa) (at 50% yield strain)	1.3	—	—	1.012
σ_{max} (low to high load rate)[a] (kPa)	80–100	85–95	—	—
ν, Poisson's ratio	0.3–0.4	—	0.496	0.49
A_0 (MPa)	0.12	—	0.12	0.13
A_1 (MPa)	0.0	—	0.0	0.0
A_2 (MPa)	–0.33	—	–0.33	–0.33
A_{max} (MPa)	0.12	—	0.12	0.13
φ (β) (°)	NA	NA	61	—
c (d) (kPa)	40–51	42–46	40	—
Bulk modulus, K (MPa)	—	—	1.15	1.27
K, stress ratio	—	—	1	1
α, transition parameter	—	—	0.01–0.05	—

[a]Loading rate in undisturbed tests varied from 0.174 mm/min to 0.232 mm/min, and from 0.232 mm/min to 7 mm/min for the remolded samples.

[b]Loading rate in the Munusamy and Barton (*6*) study was 60 mm/min.

NA = not applicable.

Uni-axial tests were also conducted on thermally conditioned remolded samples. As observed from the available results presented in figure 15, thermal conditioning lowered the yield stress and the maximum axial stress at failure, resulting in a narrower elastic range. The undisturbed and the remolded specimens displayed maximum axial stresses in the range of 80–100 kPa, while the thermally conditioned specimens resulted in the range of 40–50 kPa, corresponding to about a 50% decrease. These tests are continuing on thermally conditioned and aged (left to sit in room temperature over a duration) specimens to examine the possible effects of thixotrophic strength gain over time.

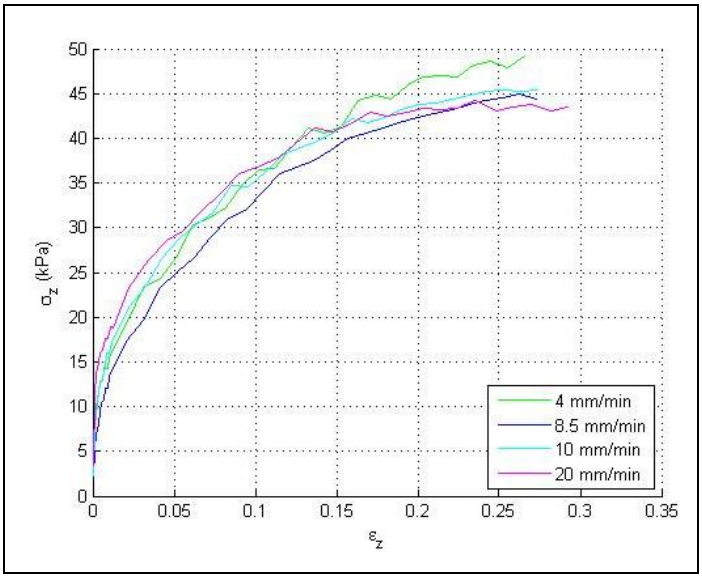

Figure 15. Uniaxial compression of remolded and thermally conditioned samples.

4.1.2.2 B2. Tri-axial Compression Test Results

Tri-axial compression tests (table 7) are conducted on undisturbed and remolded cylindrical samples at room temperature to determine the strength parameters for various material models considered. Tri-axial tests are in progress on thermally conditioned samples.

Table 7. Tri-axial compression test results.

Test Type	Mohr-Coulomb		Drucker-Prager	
	Φ (°)	**C (kPa)**	**B (°)**	**D (kPa)**
Undisturbed	42.7	22.4	60.75	39.45
Remolded[a]	~0.0	46.79	4.555	85.05

[a]Confining stress increased from 3.5 kPa to 138 kPa; the loading rate was constant at 0.232 mm/min.

Limited tri-axial compression tests were conducted initially on undisturbed clay samples to determine preliminary material input parameters to the ABAQUS software model. Shown in figure 16 are the stress-strain variations, the Mohr circle plot at failure, and the corresponding DP failure surface parameters obtained for the undisturbed clay.

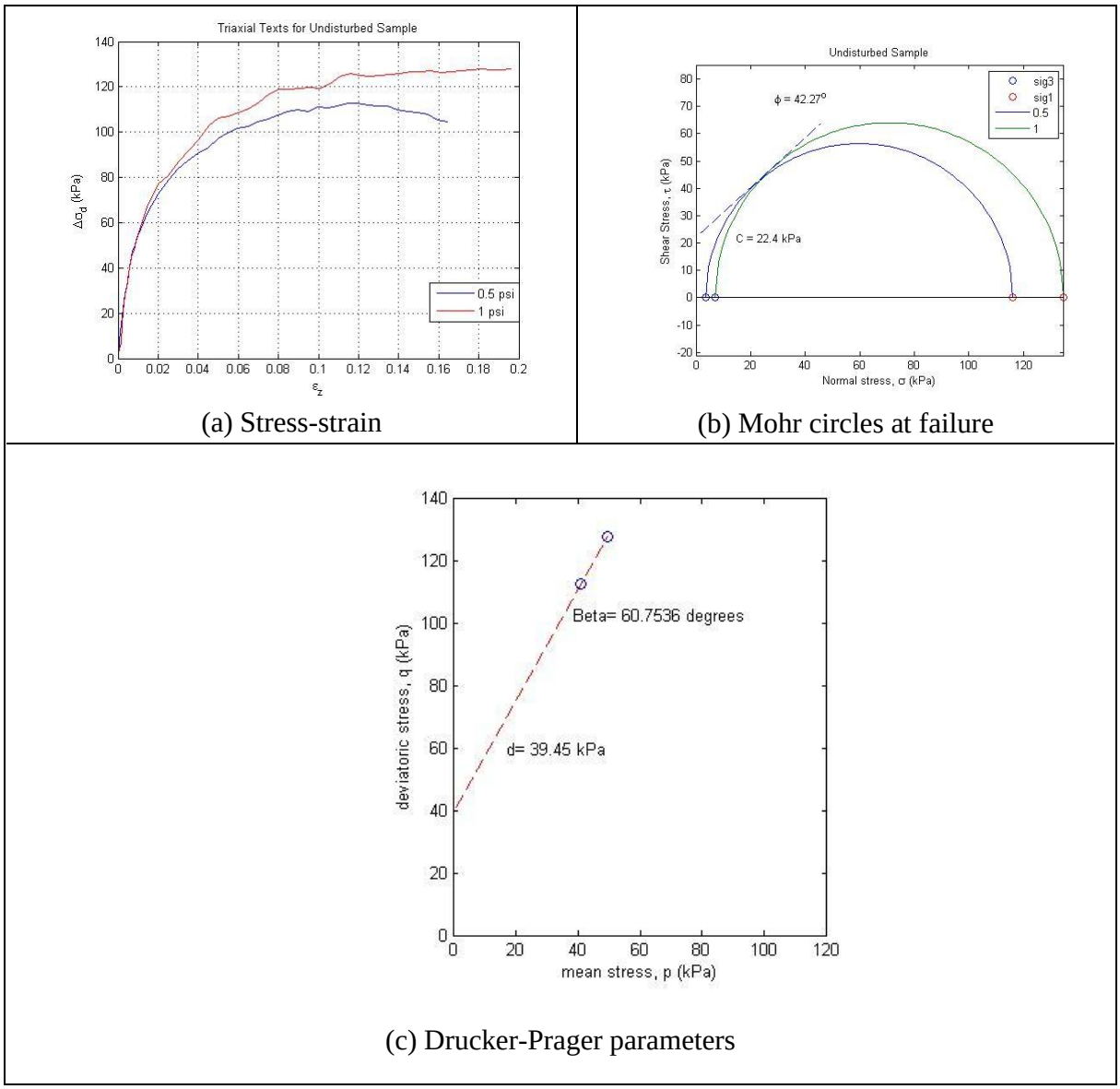

(a) Stress-strain

(b) Mohr circles at failure

(c) Drucker-Prager parameters

Figure 16. Triaxial compression of undisturbed samples for Drucker-Prager model parameters.

Similar tests were conducted using remolded cylindrical samples (figure 17). The responses of the samples in undisturbed and remolded states indicate that the process of remolding softens the clay by lowering its yield stress and the maximum stress at failure. Furthermore, the remolded sample test results indicate the lack of dependence of the material strength on mean stress

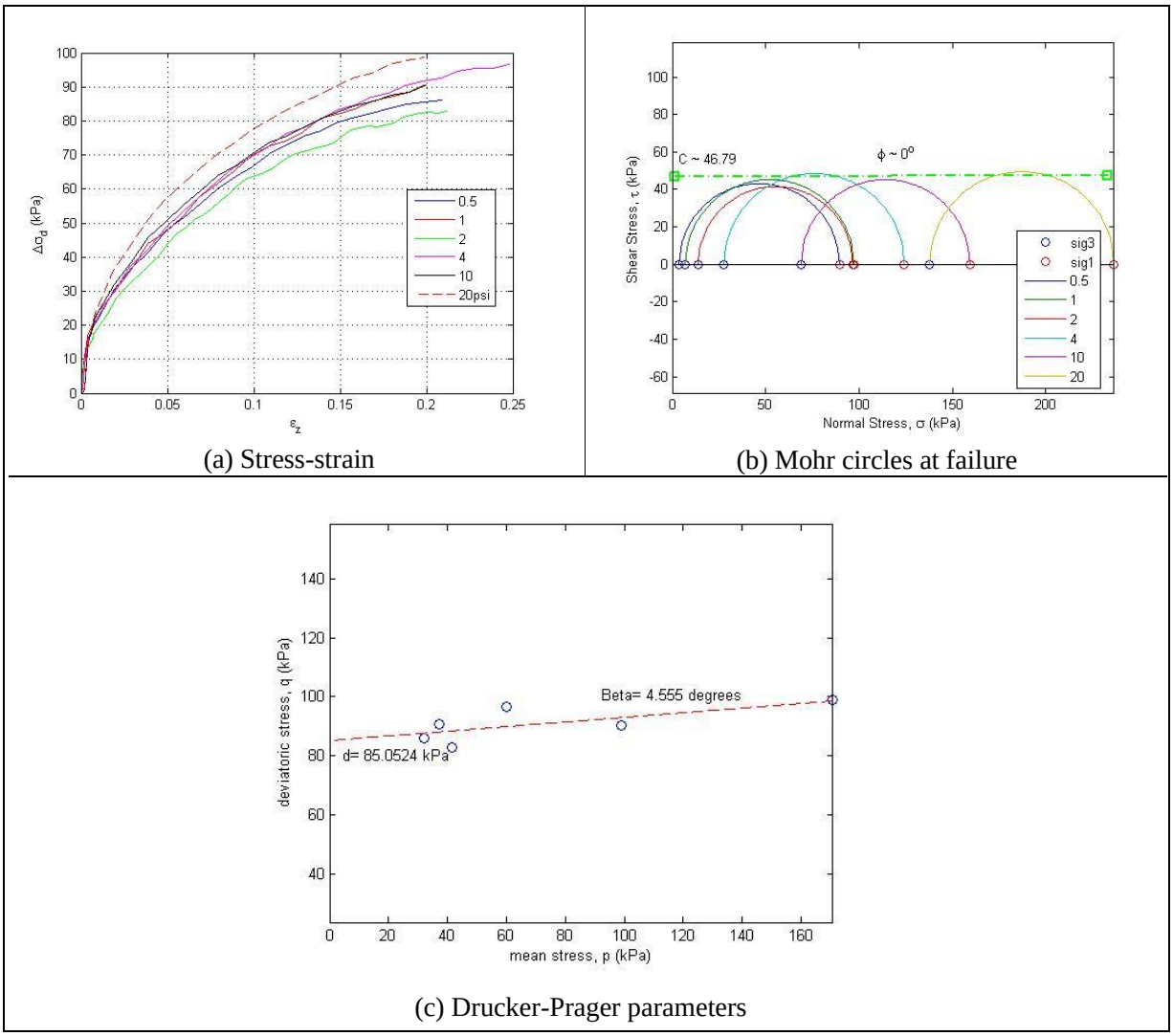

(a) Stress-strain

(b) Mohr circles at failure

(c) Drucker-Prager parameters

Figure 17. Tri-axial compression of remolded samples for Drucker-Prager model parameters.

component (confining pressure). The substantial changes in the material response in this manner have suggested that other plasticity models, such as von Mises or Modified Cam-Clay, are more suitable to model the RP clay. Although we report only the model response based on Drucker-Prager in this report, work is continuing to modify the model parameters to reflect von Mises and Cam-Clay yield behavior to be examined within the next phase of the project.

4.1.3 Constrained Compression Tests

The material properties obtained from the constrained compression tests are listed in table 8.

Table 8. Constrained compression test results and Drucker-Prager model parameters.

Property	Undisturbed	Remolded
M, initial constrained modulus (GPa)	0.33977	0.19209
λ^p, ($=\lambda/(1+e_o)$) reload modulus (1/kPa)	3.6×10^{-3}	4.9378×10^{-3}
κ^p, ($=\kappa/(1+e_o)$) unload modulus (1/kPa)	7.401×10^{-4}	9.4162×10^{-4}

The true axial stress and axial strain response for undisturbed and remolded samples are shown in figure 18.

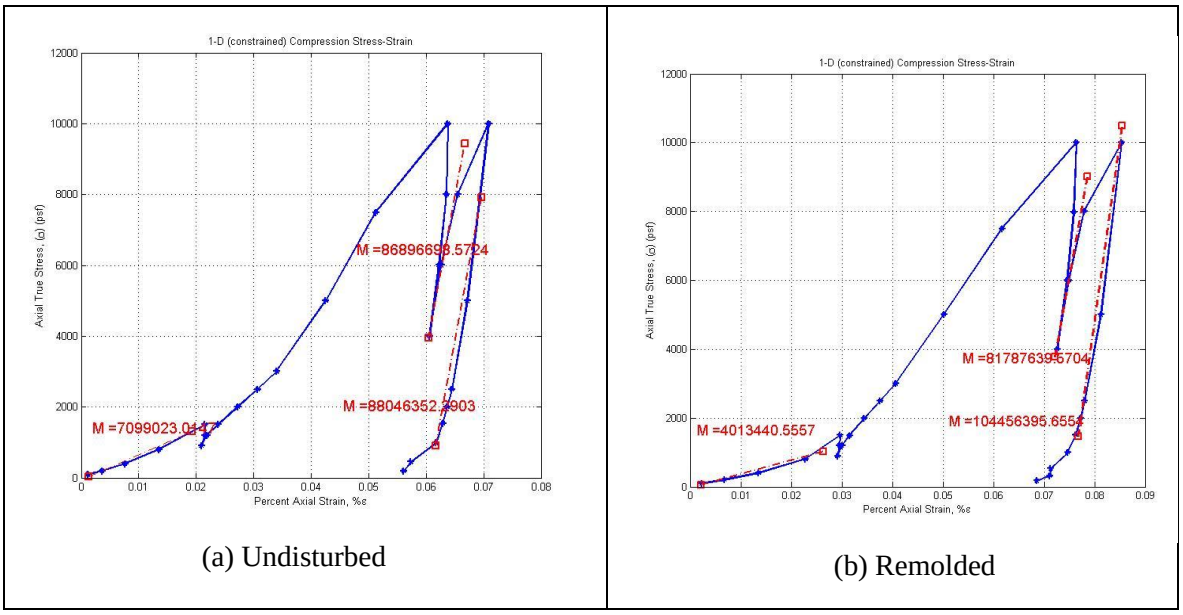

(a) Undisturbed

(b) Remolded

Figure 18. One-dimensional constrained loading (engineering strain vs. true axial stress).

The reduction in constrained modulus (M) as a result of remolding quantifies the material softening due to this process. The plastic model parameters and critical state parameters are obtained by plotting the natural log of stress and the volumetric strain, as shown in figure 19.

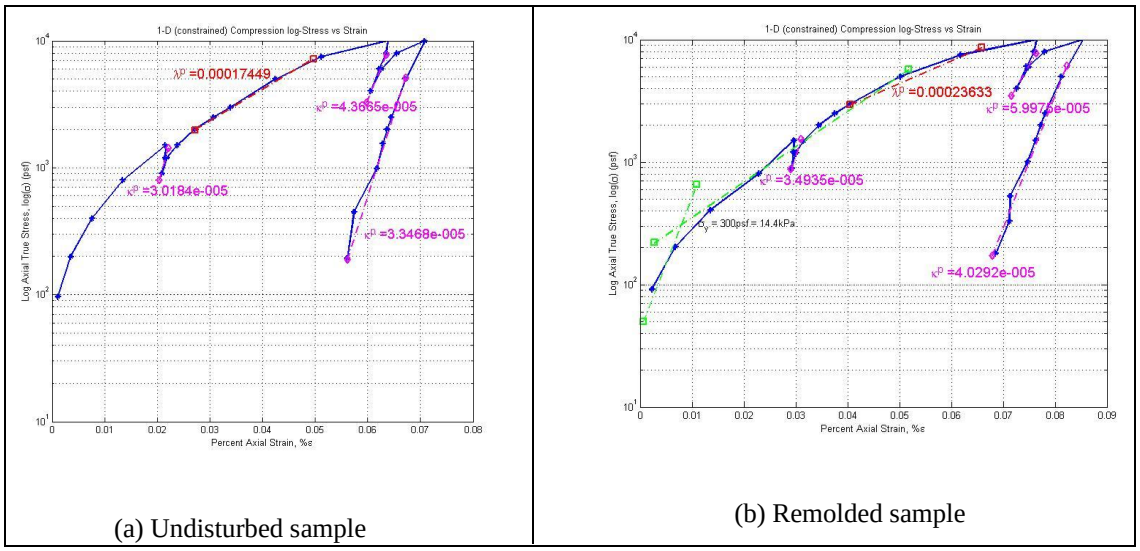

(a) Undisturbed sample

(b) Remolded sample

Figure 19. One-dimensional constrained loading (semi-log plot for model parameters).

The stress and volumetric plastic strain plots indicate a lowering in yield stress, as shown by the point of intersection of the dashed line in figure 20 for the remolded sample. This behavior is also indicative of reduction of elastic response range.

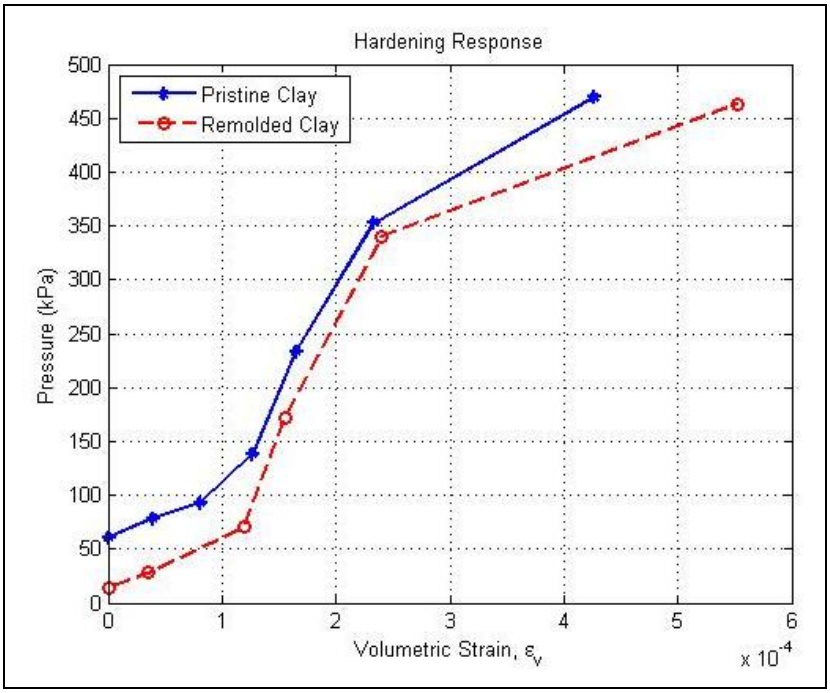

Figure 20. Hardening response of undisturbed and remolded clay samples.

4.1.4 Thermal Diffusivity Tests

The thermal responses of the mid-segment of a cylindrical RP clay sample at the core center and surface are shown in figure 21.

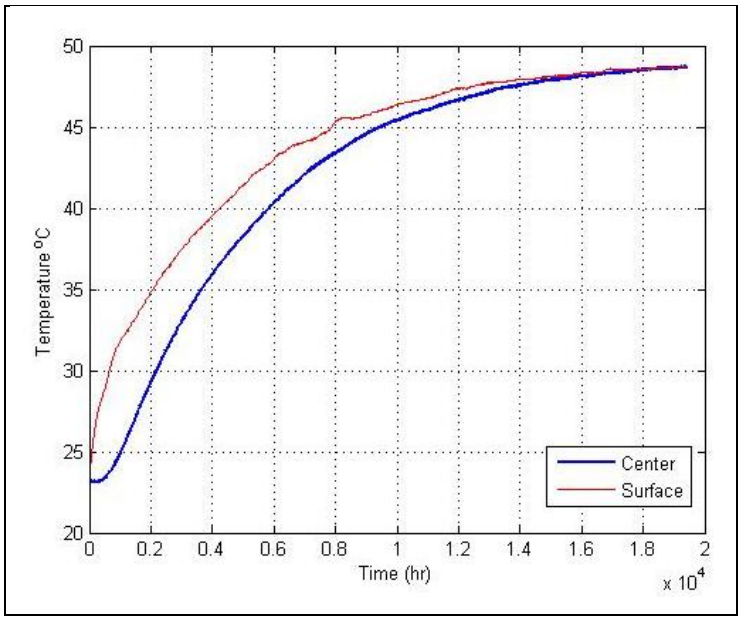

Figure 21. Center and surface temperature response of a cylindrical sample in oven.

The parameter estimation method conducted using optimization of the experimental and numerically simulated responses yielded a thermal diffusivity coefficient α equivalent to 2.1261×10^{-7} m^2/s. The experimental and the simulated thermal responses at the center and surface of the cylinder are compared in figure 22.

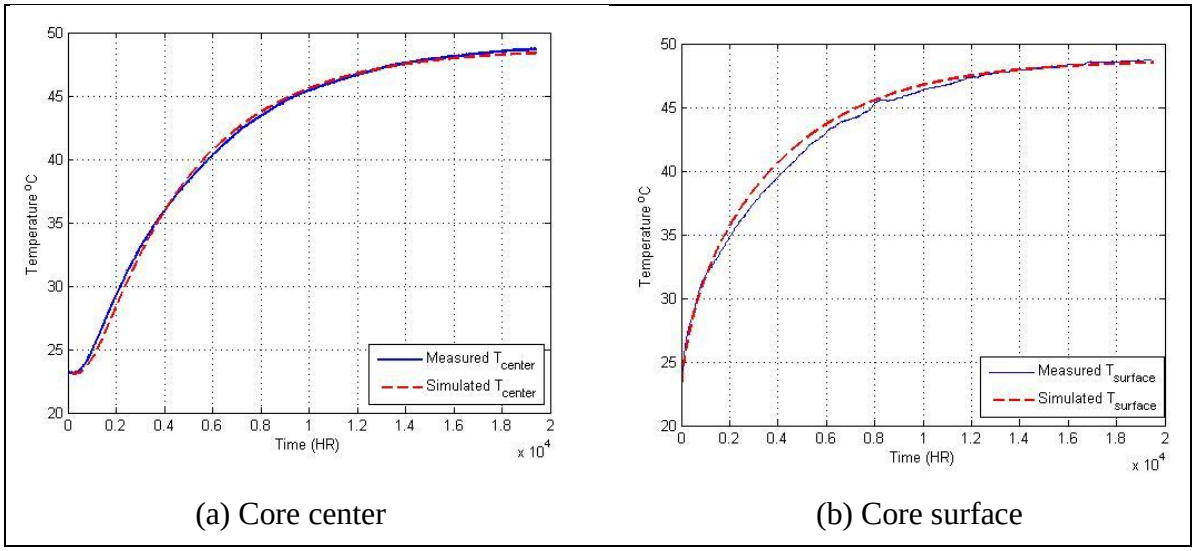

(a) Core center (b) Core surface

Figure 22. Measured and simulated temperature response of remolded cylindrical clay samples.

4.2 Results of Task 2: Construction of Numerical Model

The goal of the numerical model is to accurately predict the strain distribution in a clay body subjected to impact forces typical of those generated using the NIJ Standard 10101.04 *Ballistic Resistance of Personal Body Armor* (*1*). The model will incorporate the material parameters developed in this research program and will be verified by comparison with expected deformations generated under a drop test and impact test. The verified model will then be utilized to determine an optimum placement of the fiber-optic strain gauge array that retains sensitivity to both slow- and high-velocity impacts while minimizing the influence on deformations of the clay body. The strain variations estimated with the model will be used to determine an optimal fiber-optic strain gauge pattern. The initial stages of this process have been completed and are detailed in this section.

As previously mentioned, the NIJ standard requires the use of an RP clay body molded into a four-sided rigid box. A removable wood backing is used to assist with molding. A typical test series consists of a pretest calibration, perforation back face signature (P-BFS) test, posttest calibration, and ballistic limit test. The rear is kept in place for all tests except the ballistic limit test. The ballistic limit test examines the perforation limits for the armor under investigation. The numerical model and the resulting fiber-optic instrumentation developed here will be used only for the non-perforating calibration test and the BFS test. ABAQUS version 6.9.1 is utilized for the modeling phase of this research. The model replicates the rigid box. A steel box 6 in (152 mm) deep is assumed with the dimensions illustrated in figure 23. The model replicates the geometry of the clay portion of the box but does not explicitly model the exterior steel sides or wood rear face. The side and rear faces are assumed to be fixed normal to the plane of each face.

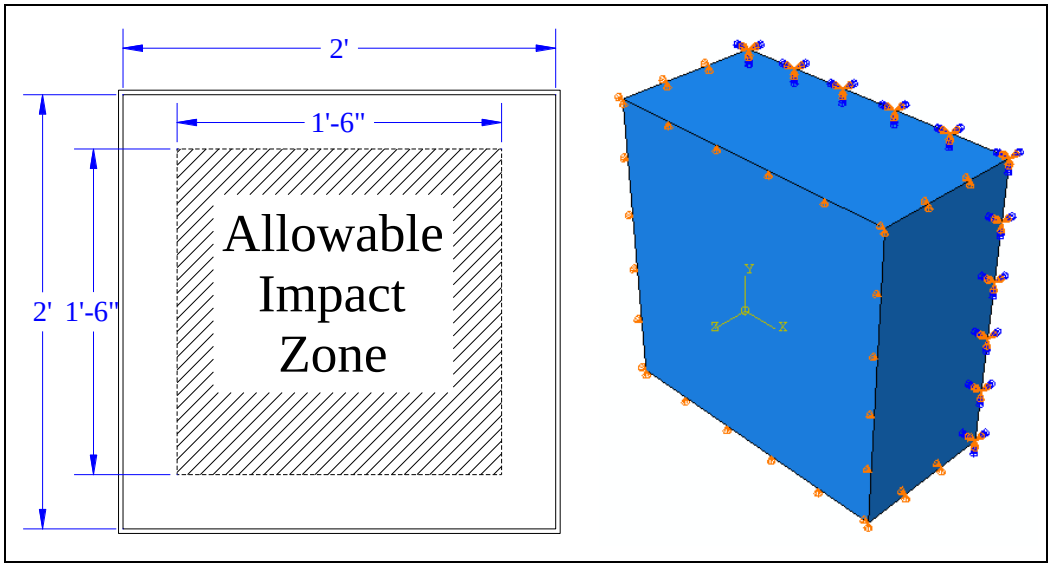

Figure 23. Clay box dimension and solid model.

The finite element model is based on the standard box, as illustrated in figure 23. Two model approaches have been conducted. The initial model consisted of a refined mesh in the center region to accurately model a center point impact. First, a non-uniform mesh is used. This model does not lend itself to multi-shot impact tests typical of the NIJ requirements. The non-uniform mesh was developed to examine the sensitivity of strain to mesh size. The second mesh consists of standard uniform rectangular elements. The uniform mesh will allow for examination of multiple impacts. The various mesh densities were examined, as shown in figure 24. An element size of 0.75 in (19 mm) was chosen to limit computational time while maintaining resolution. To minimize computational time in upcoming studies, the model will be partitioned. The full mesh is utilized at this point to allow for multiple impacts typical of calibration or P-BFS testing illustrated in figure 25.

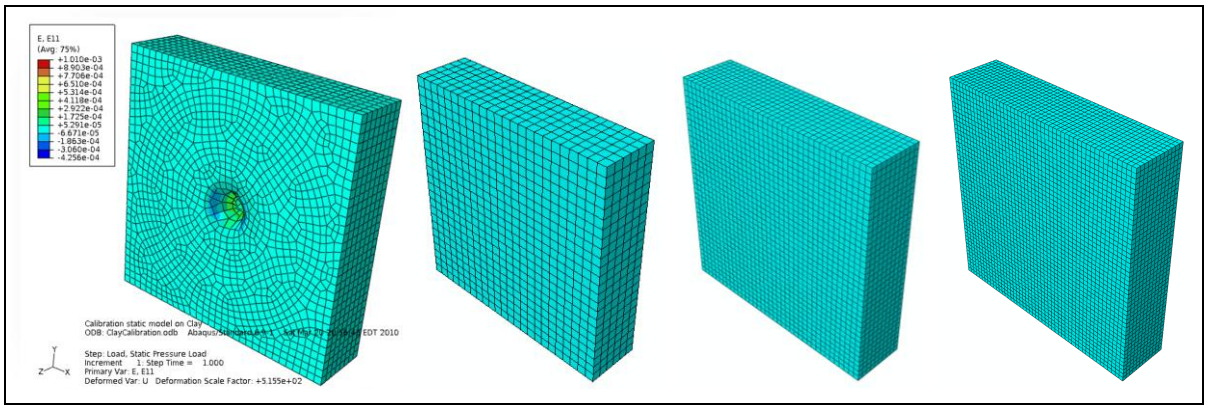

Figure 24. Mesh development.

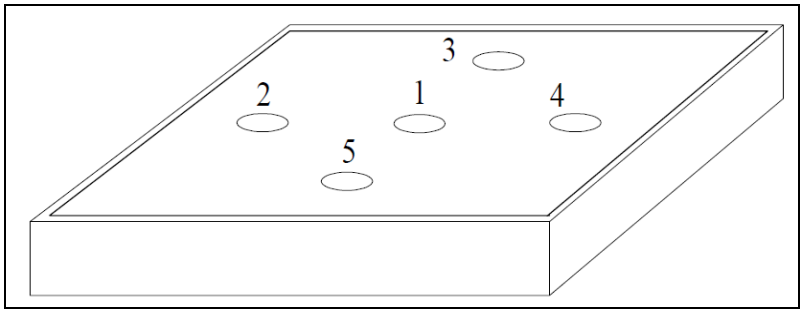

Figure 25. Pretest calibration drop series.

The initial modeling step consisted of static load evaluation and comparison with measured properties. This analysis was conducted first with an elastic model and then with an inelastic model. In the initial elastic study, a Young's modulus of 1.012 MPa (146.7 psi), Poisson's ratio of 0.49, and a bulk modulus of 1.27 MPa (184 psi) were used (table 6). These values were taken from a similar analysis described in Munusamy and Barton (*6*). The results of this phase were used to verify the software model approach. The computed deformations were on the same order

of magnitude as the expected response. The model consisted of a static application of a uniform pressure equal to the weight of the drop sphere over its diameter.

To appropriately model the impact event, the analysis method must account for the dynamics of the event as well as the inelastic properties of the material. The first phase of this analysis was to model the dynamic impact event that occurs under the calibration test. A steel drop-test sphere measuring 63.5 mm (2.50 in) was used. A density of 490 lb/ft^3 and an elastic modulus of 2.00E6 MPa (29,000 ksi) were assumed for the steel. The model is conducted with the ball in near contact (0.003 in [0.076 mm] of offset) with the surface of the clay body (figure 26). The velocity at impact is computed assuming conservation of energy and a potential energy drop height of 2.0 m. An initial velocity of 246 in/s (6.25 m/s) is used. A general contact surface interaction is used to model the interface between the clay body and the steel sphere. The model is conducted under a time-stepping algorithm.

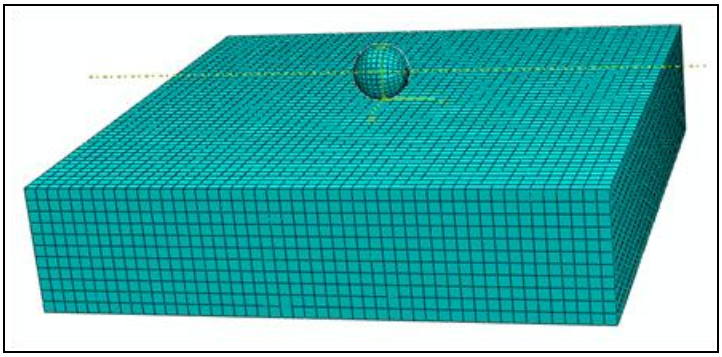

Figure 26. Ball initial location.

The nonlinear material properties are based on the material testing performed in task 1. A DP yield criterion is used. The material model properties are summarized in table 9. The hardening response is based on testing and is summarized in table 10 (follows the hardening response curve for undisturbed sample in figure 20).

Table 9. Model material properties.

Elastic modulus	955 psi (6.58 MPa)
Poisson's ratio	0.496
Density	0.0556 lb/in^3 (1.539 g/cm^3)
Yield stress	8.7 psi (60 kPa)
Angle of internal friction	61°
Flow stress ratio	1.0
Dilation angle	0°

Table 10. Hardening properties.

Yield Stress psi (kPa)	Absolute Plastic Strain
8.70 (60)	0.0
10.44 (72)	0.000119
13.92 (96)	0.000128
17.40 (120)	0.000159
20.86 (144)	0.000188
34.81 (240)	0.000263
52.21 (360)	0.000343
69.47 (479)	0.000462

4.3 Results of Task 3: Analysis of Numerical Model

The numerical model is initially verified using the NIJ calibration test procedures. Properly prepared clay should result in a permanent BFS of 19.0 +/– 2.0 mm for the ball-drop test. The initial study examines the response of the clay to the impact demand and compares the resulting deformation. The resulting maximum deformation of the impact is illustrated in figure 27. The maximum predicted deformation of the clay body using the baseline material properties identified previously is 0.84 in (21.3 mm). This predicted value is comparable to the expected deformation of 19.0 +/– 2.0 mm from the calibration test.

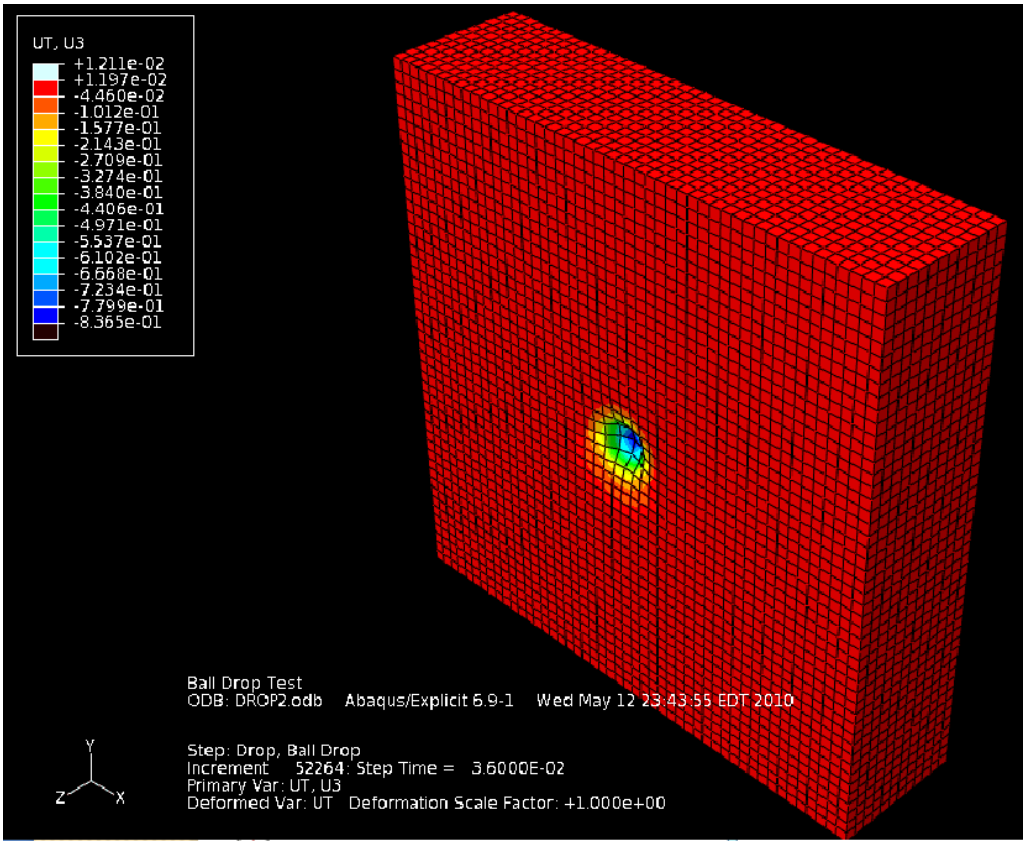

Figure 27. Deformation of clay body.

The strain profile generated in the clay needs to be examined to determine an appropriate arrangement and location of fiber-optic strain gauge array. The fiber-optic strain gauges will provide measurements in orthogonal directions in the plane of the flat surface of the clay. Due to symmetry, the strain in the X or Y can be examined. The strain in the X-direction along the centerline of the clay at increasing depths is illustrated in figure 28. Due to the flexibility and yield properties of the clay, the strain profile varies significantly through the depth of the box. At the surface, a clear reversal of strain magnitude is observed. This occurs due to the local contact of the sphere. Directly under the sphere the clay is placed in tension and away from the sphere the clay bulges outward resulting in compression on the surface. This effect is present throughout the depth of the box but decreases in magnitude with depth.

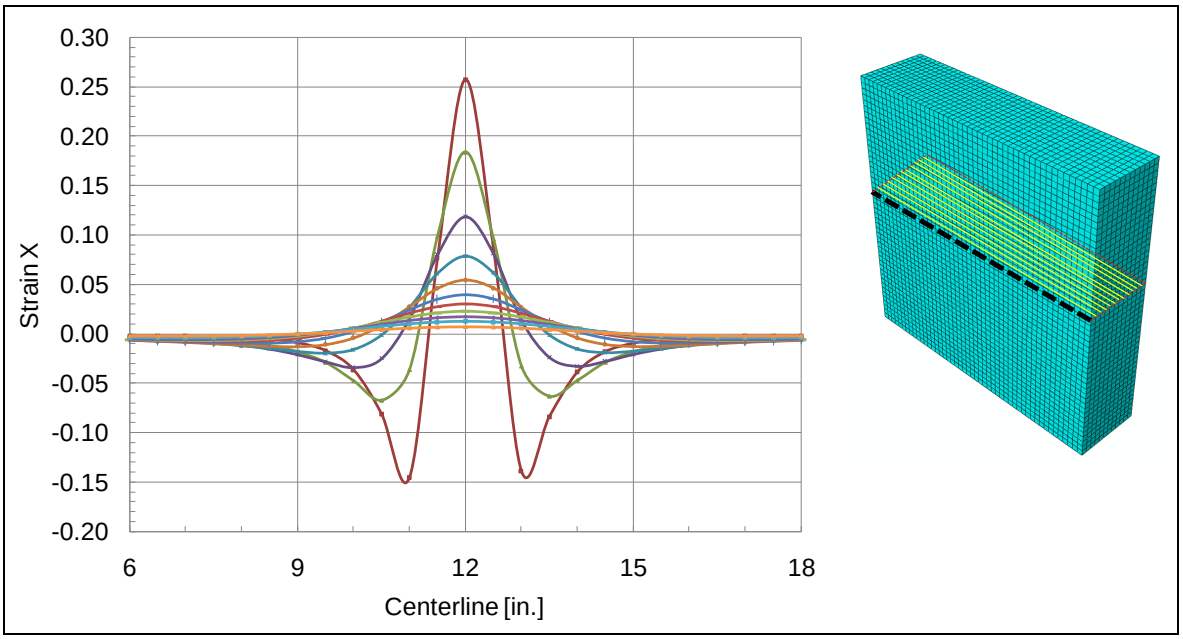

Figure 28. Strain profile along centerline.

The magnitude of the strain is of importance to the arrangement and resolution of the fiber-optic array. The predicted strain distribution along the centerline of the clay is presented in figure 29 for each 1-in (25.4-mm) depth increments of the box. Placement of the fiber-optic array at a 1-in (25.4-mm) depth will result in elevated strain levels under the calibration test. For more significant impacts, such as those generated at the P-BFS response limit, a surface deformation of 1.73 in (44 mm) is expected. These elevated impacts will result in significantly higher strain values at the surface and through the depth. The BOTDR fibers are expected to be capable of a maximum strain of 0.040 and a resolution of 10 με. As illustrated in figure 29, a mid-depth placement of the fiber array at 3 in (76.2 mm) below the clay surface should provide adequate protection from the high surface strains while still providing the required resolution.

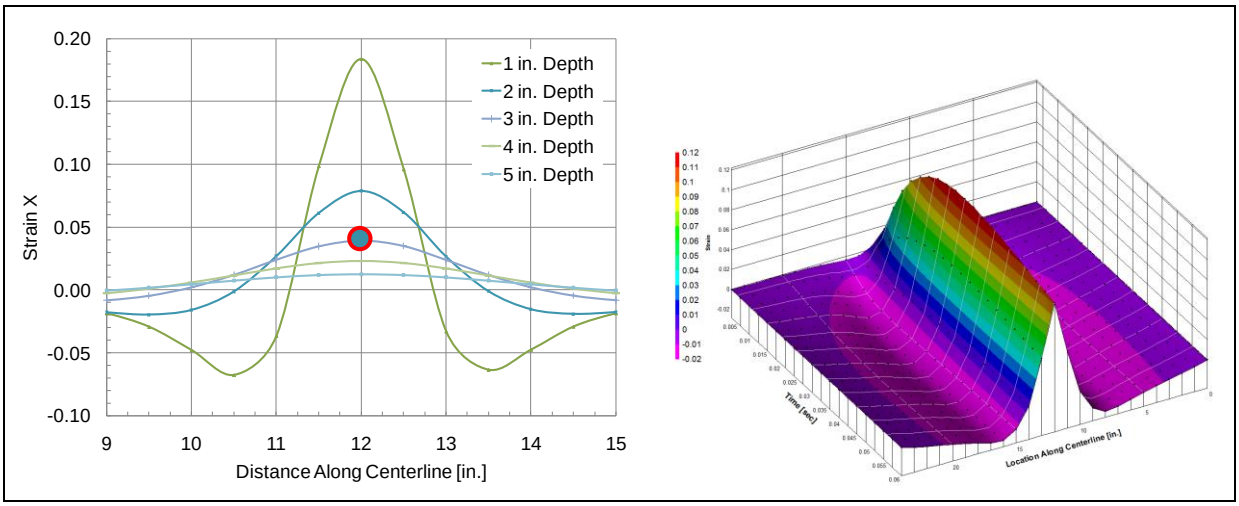

Figure 29. Strain profile along centerline at specific depths.

An in-depth evaluation of the strain profile within the section is ongoing. The results of this study will be used to determine an appropriate arrangement for the fiber-optic array. The fiber-optic array will consist of a grid arrangement with each intersection bonded. This will allow for localized strain measurements at discrete locations within the clay body. Three potential arrangements are illustrated in figure 30.

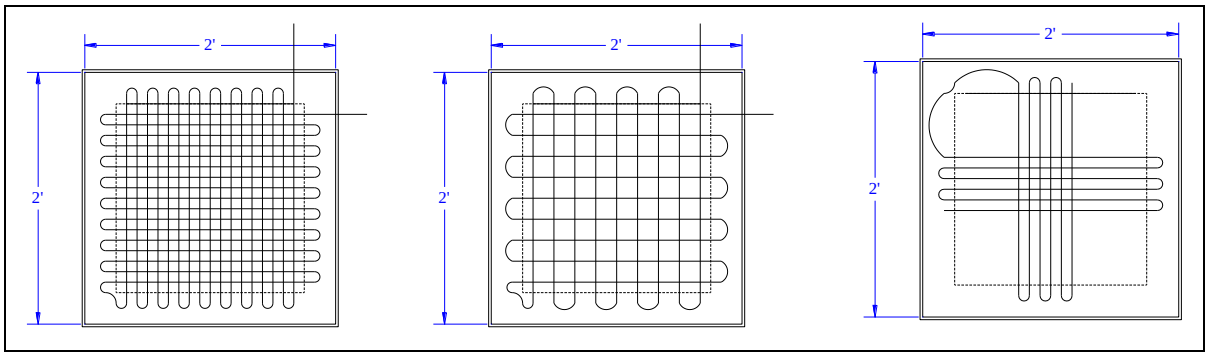

Figure 30. Fiber-optic array ideas.

One of the shortcomings of the NIJ methods is the inability to assess the impulse energy of the impact event. The procedure is limited to the resulting plastic deformation generated. The time duration over which the deformation event occurs could vary significantly based on the type of armor used. This variation could have a significant influence on the lethality of the impact. For example, two armors could result in the same BFS. If, however, one armor generates the BFS over a much shorter duration, the resulting energy imparted could be much less. The NIJ procedure does not provide an assessment of this variation. To enhance the results of the NIJ test procedure, the fiber-optic array will be used in conjunction with the finite element results to analytically assess the energy imparted during the test. The following procedure is proposed:

1. The NIJ P-BFS test will be conducted with the fiber-optic strain gauge array installed.
2. The characteristic strain from the fiber array will be measured vs. time (figure 31a).
3. The FE model will be used to determine a verified relationship between the characteristic strain and the surface pressure imparted. This relationship will be used to convert the measured fiber strain to the expected surface pressure (figure 31b).
4. Finally, the surface pressure vs. time will be determined and integrated to determine the impulse energy of the impact event (figure 31c).

The actual relationships are under development and will require further study. A characteristic strain will need to be determined. This may represent the peak strain or a portion of the strain profile measured at the fiber-optic strain gauge level.

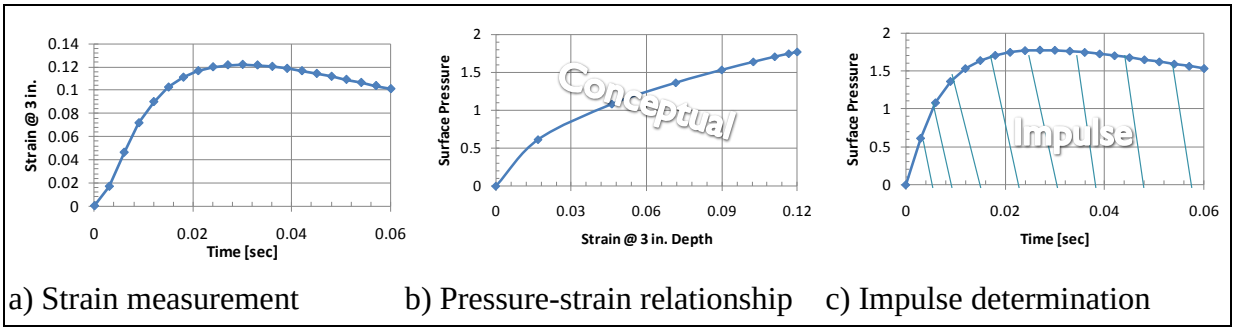

a) Strain measurement b) Pressure-strain relationship c) Impulse determination

Figure 31. Impulse measurement technique.

5. Ongoing Modeling Efforts

The following modeling efforts are underway and are expected to be completed within the project schedule.

1. Integration of Measured Material Properties. In addition to Drucker-Prager, more suitable material models are being developed. The influence of rate effects, confinement, and other yield criteria will be incorporated in the solution of these models.
2. Identify Influence of Thermal Sensitivity on Strain Response. The variation in material characteristics under thermal variations will be examined. The NIJ specification requires testing under an elevated temperature. This could have a significant influence on the response of the clay body and, potentially, the properties of the fiber-optic array.

   Table 11 summarizes the plan of continuing material testing necessary to assist the modeling efforts in items 1 and 2.

Table 11. Plan of continuing material tests to assist improved modeling.

Test	Description	Required Parameters Obtained for Each Constitutive Model of the FEA		
		Modified Drucker-Prager	von Mises	Modified Cam-Clay
Uni-axial compression	Variable deformation rate and zero confining pressure	E, σ_y, σ_{max}, post-failure response, stress exponent (n)	E, σ_y, σ_{max}, post-failure response, stress exponent (n)	E, σ_y, σ_{max}, post-failure response, stress exponent (n)
Tri-axial compression	Variable deformation rate and variable confining pressure	Elastic: E Strength: d, β Yield	Elastic: E Strength: $\sigma_y/2$	Elastic: E Strength: M' Yield
Constrained compression	Constant load in time	Elastic: M Hardening: P-ε_v	Elastic: M Plastic/elastic strains	Elastic: M Plastic/elastic response: λ and κ
Nondestructive testing	Ultrasonic Bender element Resonant column	-Wave velocities: V_p and V_s -Elastic properties: E_{max}, G_{max}, K, and ν -Dynamic response: G_{max} and D_{min} (attenuation) -Dynamic G vs. elastic strain -Thixotrophic strength and stiffness variation over time		

3. Examine the Influence of Box Geometry and Clay Thickness. It is fairly easy to account for the effects of box geometry and clay thickness in the model. Box size variation is currently being examined. Variations in thickness can also be examined. If further information on these effects is needed, a range of geometries and thicknesses would be useful to bound the scope of the parametric study.

4. Examine Sensitivity to Material Model Parameters. The sensitivity of material model parameters on the strain distribution and deformation will be examined.

5. Examine Rate Sensitivity of Strain Profile Within Clay. The rate sensitivity of the model will be examined by comparing the deformation response from impact of a comparable energy projectile. A higher velocity, smaller mass sphere will be used and compared with deformation measured from an actual impact test on the clay body in the laboratory.

6. Examine Influence of Embedded Optical Fiber on Clay Response. The influence of the fiber-optic strain gauge array on the BFS will be assessed. It is imperative that the fiber-optic array not influence the BFS measurements. This will ensure that future tests conducted with the array installed can be compared to the historical data generated. This will be attempted using FEM studies and through physical verification under the calibration test. The goal will be to determine a location and quantity of fiber that can be used that will not affect the BFS of the shot at the failure level while still providing adequate strain resolution. The validity of the model can then be verified by physically conducting tests with and without the final arrangement of fibers and comparing the difference in the BFS between the two samples.

7. Examine Influence of Other Embeds on Clay Response. The inclusion of holes or fissures in the clay bed can be examined; however, the compressibility of the actual air voids may be difficult to verify. A general sensitivity study could be conducted to examine how void size can alter the BFS.
8. Determine Strain Distributions Under Kill Shot Level. The strain distribution at the deformation response limit of 44 mm will be examined, as will the magnitude and distribution of strain through the depth of the clay body.
9. Develop Correlation between Strain and Surface Pressures. A relationship will be developed for the final model that will correlate the surface stress and internal strain. This relationship will be used for impulse energy estimation.

All of the tests are repeated in adequate numbers to determine statistically sound mean values of all the measurements and alleviate mathematical spread. All objectives necessary to carry on to the next phase of the project were completed.

6. References

1. National Institute of Justice (NIJ) Standard 10101.04. *Ballistic Resistance of Personal Body Armor*, Section 5.7.5; U.S. Department of Justice: Washington, DC, September 2000.
2. ASTM D2166-06. Standard Test Method for Unconfined Compressive Strength of Cohesive Soil. *Annu. Book ASTM Stand.* **2006**.
3. ASTM D2850-03a. Standard Test Method for Unconsolidated-Undrained Triaxial Compression Test on Cohesive Soils. *Annu. Book ASTM Stand.* **2003**.
4. ASTM D2435-04. Standard Test Methods for One-Dimensional Consolidation Properties of Soils Using Incremental Loading. *Annu. Book ASTM Stand*. **2004**.
5. Schofield, A. N.; Wroth, C. P. *Critical State Soil Mechanics*; McGraw-Hill: New York, 1968; p 310.
6. Munusamy, R.; Barton, D. C. *Behaviour of Roma Plastilina Upon Blunt Projectile Impact*, DYMAT 2009 – 9th International Conference on the Mechanical and Physical Behaviour of Materials Under Dynamic Loading, Brussels, Belgium, 7–11 September 2009; Vol. 1.

NO. OF
COPIES ORGANIZATION

1 (PDF) DEFENSE TECHNICAL INFORMATION CTR
DTIC OCA
8725 JOHN J KINGMAN RD
STE 0944
FORT BELVOIR VA 22060-6218

1 (PDF) DIRECTOR
US ARMY RESEARCH LAB
RDRL CIO LL
2800 POWDER MILL RD
ADELPHI MD 20783-1197

1 (PDF) GOVT PRINTG OFC
A MALHOTRA
732 N CAPITOL ST NW
WASHINGTON DC 20401

1 (PDF) USARL
RDRL SLE
R FLORES
WSMR NM 88002-5513

ABERDEEN PROVING GROUND

1 (HC) DIR US ARMY EVALUATION CTR HQ
TEAE SV
P A THOMPSON
2202 ABERDEEN BLVD 2ND FL
APG MD 21005-5001

4 (2 HC 2 PDF) DIR USARL
RDRL SL
J BEILFUSS
P TANENBAUM
RDRL SLB A
M PERRY (PDF)
RDRL SLB W
M MENTZER (PDF)